The *Toxoplasma* monocarboxylate transporters are involved in the metabolism within the apicoplast and are linked to parasite survival

Hui Dong, Kai He, Jiong Yang, Wen-Bin Zheng, De-Hua Lai, Jing Liu, Hui-Yong Ding, Rui-Bin Wu, Kevin M. Brown, Geoff Hide, Zhao-Rong Lun, Xing-Quan Zhu, Shaojun Long ✉

National Key Laboratory of Veterinary Public Health Security, College of Veterinary Medicine, China Agricultural University, Beijing 100193, China • National Animal Protozoa Laboratory and School of Veterinary Medicine, China Agricultural University, Beijing 100193, China • State Key Laboratory of Biocontrol, School of Life Sciences, Sun Yat-Sen University, Guangzhou 510275, China • College of Veterinary Medicine, Shanxi Agricultural University, Taigu 030801, Shanxi Province, China • Department of Microbiology and Immunology, University of Oklahoma Health Sciences Center, Oklahoma City, Oklahoma, USA • Biomedical Research and Innovation Centre and Environmental Research and Innovation Centre, School of Science, Engineering and Environment, University of Salford, Salford, M5 4WT, UK

Abstract

The apicoplast is a four-membrane plastid found in the apicomplexans, which harbors biosynthesis and organelle housekeeping activities in the matrix. However, the mechanism driving the flux of metabolites, in and out, remains unknown. Here we used TurboID and genome engineering to identify apicoplast transporters in *Toxoplasma gondii*. Among the many novel transporters, we show that one pair of apicomplexan monocarboxylate transporters (AMTs) appears to be evolved from the putative host cell that engulfed a red alga. Protein depletion showed that AMT1 and AMT2 are critical for parasite growth. Metabolite analyses supported the notion that AMT1 and AMT2 are associated with biosynthesis of isoprenoids and fatty acids. However, stronger phenotypic defects were observed for AMT2, including in the inability to establish *T. gondii* parasite virulence in mice. This study clarifies, significantly, the mystery of apicoplast transporter composition and reveals the importance of the pair of AMTs in maintaining the apicoplast activity in apicomplexans.

eLife assessment

This **important** study identifies two new transporters of the apicoplast, a non-photosynthetic organelle of apicomplexan parasites. In its current state, evidence is **incomplete**, as it only partially reveals how **important** those transporters are and as it does not address the metabolic function for the parasite. The results should be of interest to parasitologists and eukaryotic cell biologists.

Introduction

The phylum Apicomplexa encompasses thousands of intracellular parasites, including *Plasmodium*. spp., the notorious agent of malaria, and *Toxoplasma gondii*, the highly successful parasite that infects almost all warm-blooded animals and humans (Plattner and Soldati-Favre, 2008). It is believed that apicomplexan evolution included two key independent, and sequential, endosymbiotic events, finally leading to the common ancestor of the chromalveolates (e.g. alveolates, heterokonts, oomycetes and Cryptomonads) (Cavalier-Smith, 1999; Gould et al., 2008; Janouskovec et al., 2010). This ancestor eventually gave rise to the apicomplexans, most of which still contain, a secondary non-photosynthetic plastid, the apicoplast (McFadden and Yeh, 2017; Obornik et al., 2009; Salomaki and Kolisko, 2019). Therefore, the apicoplast membranes have evolved from the red algal plastid, the algal plasma membrane and the host endomembrane when counting from the innermost to outermost membranes of the apicoplast (Gould et al., 2008; McFadden and Yeh, 2017). This heavily compartmentalized feature poses great challenges for metabolic integration of the organelle within the parasites and, in particular, the transport of metabolites across these membrane systems.

The apicoplast houses essential biosynthetic pathways, which include the fatty acid synthesis type II (FASII), methylerythritol phosphate (MEP) pathways, Fe-S cluster and (partial) heme biosynthesis pathway (Fata and Rabuzzi, 1988; Kloehn et al., 2021; Krishnan et al., 2020; Ralph et al., 2004; Tjhin et al., 2020). They are able to make critical components of fatty acids and isoprenoid precursors, for the parasites in *T. gondii* and *Plasmodium falciparum* (McFadden and Yeh, 2017; Ramakrishnan et al., 2012; Striepen, 2011; Vaughan et al., 2009; Yeh and DeRisi, 2011). Moreover, the apicoplast maintains housekeeping activities for genome replication, transcription and translation (Low et al., 2018; McFadden and Roos, 1999). Accordingly, it requires adequate supplies of carbon molecules, energy, reducing equivalents, cofactors, amino acids, nucleotides as well as inorganic ions, to feed the biosynthetic pathways and plastid maintenance activities in the matrix (Kloehn et al., 2021; McFadden and Yeh, 2017; Ralph et al., 2004). However, compared to plant plastids, the nature of the channels and transporters in the apicoplast remains obscure.

The apicoplast biosynthetic pathways were characterized through a homology/bipartite signal-based approach (Foth et al., 2003; Ralph et al., 2004). A similar approach was utilized to identify phosphate translocators in *T. gondii* (i.e. *Tg*APT1) and *P. falciparum* (i.e. *Pfi*TPT and *Pfo*TPT), and a two-pore channel TPC in *T. gondii*. These transporters are capable of supplying phosphorylated carbons, (Brooks et al., 2010; Fleige et al., 2007; Karnataki et al., 2007; Lim et al., 2010; Mullin et al., 2006), and calcium to the apicoplast (Li et al., 2021). It was proposed that an early step in the endosymbiotic event was to integrate transporters that exchange metabolites across the membranes (Cavalier-Smith, 2000; Weber et al., 2006). Consistent with that, studies demonstrated that 57-58% of the chloroplast transporters have an origin in the putative host cell in the first endosymbiosis while 20-30% are from bacteria (Karkar et al., 2015; Tyra et al., 2007). It is plausible that a complex transporting system was produced in the evolution of the secondary plastid (i.e. the apicoplast).

Recent studies suggested that we still do not know the major source of pyruvate required for the biosynthesis pathways in the apicoplast of *T. gondii* and *P. falciparum* (Swift et al., 2020; Xia et al., 2019). Thereafter, identifying the apicoplast transporter composition and their functions is critical for an understanding of how these transporters evolved and how the organelle maintains its metabolic and housekeeping activities. In this study, we utilized the apicomplexan model organism *T. gondii* to screen apicoplast membrane proteins, identified from available computational and proteomic information (Barylyuk et al., 2020; Boucher et al., 2018) and from our APT1-TurboID proximity proteomic candidates, and discovered

several novel apicoplast transporters. Among the many transporter candidates, one pair of monocarboxylate transporters (AMTs) appeared to have evolved from the putative host cell involved in the evolution of the secondary plastid. Detailed analyses support association of the AMTs with the apicoplast biosynthesis pathways likely by supplying the pathways with substrates. This study opens up the possibilities of tackling difficult questions of substrate transport and especially for the pair of monocarboxylate transporters in *T. gondii* and in other members of this phylum of deadly parasites.

Results

Discovery of novel transporters in the apicoplast of *T. gondii*

To identify apicoplast transporter proteins in *T. gondii*, we first analyzed candidates identified in recent studies using combined proteomic and computational analyses in *T. gondii* and *P. falciparum* (Barylyuk et al., 2020; Boucher et al., 2018). The hyperplexed localization of organelle proteins (hyperLOPIT) assigned 129 proteins to the apicoplast (Barylyuk et al., 2020), of which three proteins were likely transporters, i.e. APT1 (Transmembrane Domain, TMD=6), one major facilitator superfamily (MFS) transporter (TGME49_309580) (HAP1, hypothetical apicoplast protein 1) and one hypothetical protein (TGME49_267690) (HAP2) (Table S1). We also mined an apicoplast proteomic dataset obtained by ACP-BioID in *P. falciparum* (Boucher et al., 2018), which reported 16 TMD≥6 protein candidates, and two additional candidates annotated as ABC transporters (TMD<6). We identified the orthologues in *T. gondii* using the *P. falciparum* candidates (Boucher et al., 2018; Sayers et al., 2018), resulting in 8 candidates in *T. gondii*. They were temporarily named as HAP3-9 (Table S1). Taken together, these datasets provided only limited numbers of candidate transporters.

To better define the repertoire of apicoplast transporters, we employed a biotin proximity labeling strategy that is useful for defining organelle proteomes. A promiscuous biotin ligase tag called TurboID was endogenously fused with APT1, using a CRISPR approach (Table S2-4) (Branon et al., 2018; Brooks et al., 2010; Long et al., 2018). The apicoplast Acetyl-CoA carboxylase 1 (ACC1) is a strongly biotinylated protein (Zuther et al., 1999), which might provide a clear and strong streptavidin labeling at the apicoplast (Figure 1A). Though the streptavidin signal and the protein itself were slightly diffused (Karnataki et al., 2007), APT1 was reported to mainly localize to four of the apicoplast membranes (Karnataki et al., 2007). Many additional bands present on the APT1-TurboID lane were likely to be the apicoplast proteins (Figure 1B). The resultant mass-spectrometry datasets (N=3 for each) (Dataset S1) were analyzed by comparing the APT1-fusion to the parental line (Figure 1C and Table S5). This analysis showed that APT1 itself has the highest *p*-value associated with its enrichment in the TurboID line, as would be expected for a bait protein. The TMD candidates (TMD≥6 and 2≤TMD<6) were evenly distributed on the volcano map plotted by fold changes against *p*-values in a similar pattern to the distribution of known apicoplast proteins (Figure 1C and Table S6). These features suggested that APT1-TurboID had enriched apicoplast proteins. Thereafter, we compiled a list of the hits in order of TMD numbers, and selected all transporter candidates (including carriers) and hypothetical proteins (TMD≥6) as candidates (Table S7). These candidates were merged with the previously described ones (HAP1-9) and temporarily named as HAP10-50 (Table S8).
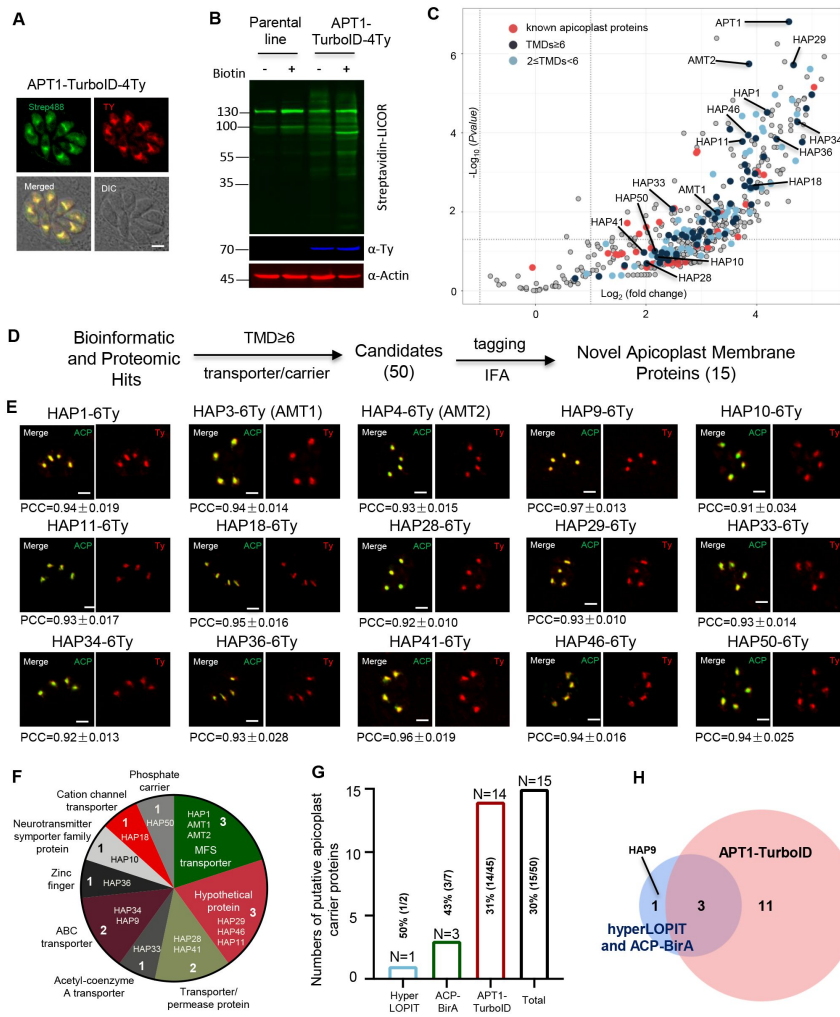
Figure 1.

Discovery of apicoplast membrane proteins

(A-B) Activity test of biotinylation of proximal proteins by APT1-TurboID-4Ty. Parasites were grown in 500 µM D-biotin for 90 min, followed by detection of biotinylated proteins (green) by streptavidin reagents on IFA (A), and on Western blots (B). Actin served as the loading control. Scale = 5 µm.

(C) Volcano plot analysis comparing the TurboID fusion to the parental line. Three replicate mass-spectrometry experiments were analyzed by the student t-test. Known apicoplast proteins (red) and candidates with different numbers of TMDs (deep and light blue were indicated, and novel apicoplast proteins were pointed out. See Dataset S1.

(D) Workflow of the discovery of novel apicoplast membrane proteins. Candidates from hyperLOPIT ([Barylyuk et al., 2020](#)), ACP-BirA ([Boucher et al., 2018](#)) and APT1-TurboID (this study)

were screened by epitopte tagging and IFA.

(E) Confocal co-localization of HAP-6Ty with the apicoplast marker ACP, showing confocal imaging of HAP-6Ty (red) and ACP (green), and Pearson Corelation Coefficiency (PCC). The PCC values over the merged fluoresent foci for candidate proteins and ACP were analyzed by a co-localization and ROI intensity analysis module in the NIS Elements AR software and shown with mean ± SEM (N=6 for each). Scale = 5 µm.

(F-H) Summary and comparison of the screening from three datasets. The putative transporters are grouped into diverse types (F) and identified from three different datasets (G), which shared three novel proteins, as shown by the venn diagram (H). Three independent experiments were performed with similar outcomes (A, B, E).

After the above candidate selections, as described in our workflow ([Figure 1D](#)), we compiled a list of 50 candidates (HAP1-50) for endogenous tagging and IFA analysis in *T. gondii*. We successfully generated endogenous HAP-6Ty fusion lines (46 HAPs) using a CRISPR-Cas9 tagging approach (Figure S1A and Tables S2-4), as described in our previous study ([Long et al., 2017b](#)). Indirect fluorescence assay (IFA) showed that many HAP-6Ty fusions were localized to foci inside the parasites, resembling the position of the apicoplast location

(Figure S1A), whereas some candidates were likely to be in the cytosolic vesicles (e.g. HAP13, HAP30, HAP35), the apical region (e.g. HAP19) or other structures (e.g. HAP22) (Figure S1B). Further analysis was performed by co-localization of the fusions with an apicoplast marker ACP, which showed that many of the foci had no or only partial co-localization with ACP (Figure S2A). However, strict analyses clearly identified 15 HAP fusions that were almost perfectly co-localized with ACP (Figure 1E).

Of the 15 novel apicoplast membrane proteins, we identified in *T. gondii* that 12 proteins are annotated as putative transporters or carriers in TOXODB, and 3 are annotated as hypothetical proteins (TMD≥6) (Figure 1F and Table S9). These novel proteins included 1 from hyperLOPIT, 3 from ACP-BirA and 14 from our APT1-TurboID (Figure 1G), among which three of these proteins shared between the APT1-TurboID and the combinations of hyperLOPIT and ACP-BirA (Figure 1H). Collectively, TurboID proved to be a reasonably robust approach for the identification of putative apicoplast transporters.

Novel transporters are mostly conserved in the Apicomplexa

To determine if the apicoplast transporters we identified in *T. gondii* are conserved in the Apicomplexa, we searched for orthologues of these novel proteins in different species, as shown in Fig. 2A-B. The chromalveolate hypothesis proposed a plastid origin in a common ancestor of a single red alga, which unites the Alveolates with the chromists (Cavalier-Smith, 1999). We identified orthologues in species belong to the taxa using a powerful Hidden Markov Model (HMM) profiling strategy. The best hits (the cutoff E-value: 1x10-7) remained on the list of resultant orthologues in these species, which were then used for conservation analyses in the ComplexHeatmap package in R (v4.2.0) (Gu et al., 2016) (Table S10, which contains the hits with E-values). The conservation heatmap showed that proteins with conserved transport domains (HAP1, 3, 4, 9, 10, 28, 33, 34, 41 and 50) are mostly conserved in the Apicomplexa (Figure 2A), including the Gregarina and *Cryptosporidium* that have lost the apicoplast. Further analysis revealed that most orthologues with the exception of HAP3 and HAP4, can be identified in green algae, red algae and plants (Figure 2B). As the red alga is considered to have given rise to the ancestor of the secondary plastid (Gould et al., 2008; Janouskovec et al., 2010), the results thus indicated that those transporters were possibly derived from the red alga. However, further analysis would be required to clarify their origins, as shown for chloroplastid transporters (Karkar et al., 2015).
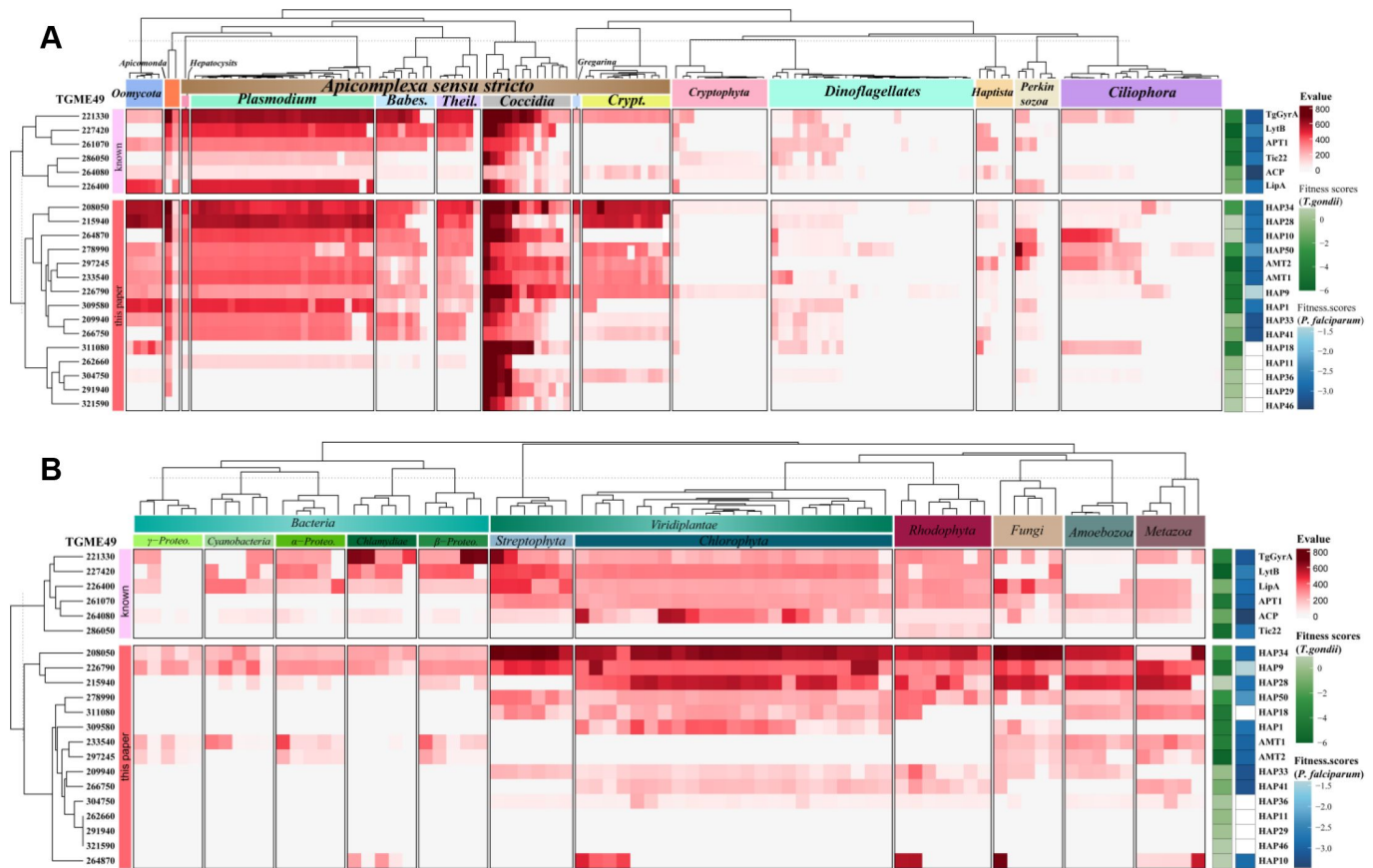
Figure 2.

Conservation analysis of putative transporters

(A-B) Heatmap indicating conservation of known apicoplast proteins and newly identified proteins among chromalveo-lates (A), red alga, green alga, plants, fungi, metazoa and bacteria (B). The conservation was scaled by a heat bar (red) with E-values for putative orthologues of the listed proteins (see Dataset S2). ToxoDB protein numbers (left) and protein (temporary) names (right) are shown. Their sequences were searched for orthologues using the Hidden Markov Model (HMM) (E value<E-7) and the best orthologue was used for the heatmap analysis in ComplexHeatmap package in R. Parasite fitness scores were shown on the right with the green heat bar for *T. gondii* (ToxoDB)(Sidik et al., 2016) and the blue bar for *P. falciparum* (PlasmoDB)(Zhang et al., 2018). The tree dendrogram across the genes were clustered according to the euclidean distance using UPGMA method. The species tree (top) shows phylogenetic relationships and major clades: *Theil.*, *Theileria*; *Babes*, *Babesia*; *Crypt.*, *Cryptosporidium*; *Proteo*, *Proteobacteria*.

AMT1 and AMT2 might have critical roles in metabolic integration of the apicoplast

Several transporters, such as HAP1, 3, and 4 and 34 and 50, are predicted to be essential in *T. gondii* and in *P. falciparum* (Figure 2A-B, and Table S9 contains the *P. falciparum* orthologues with fitness scores) (Sidik et al., 2016; Zhang et al., 2018). The analyses with InterProScan showed that three of these transporters (HAP1, 3 and 4) belong to the major facilitator superfamily (MFS) (Figure S2B). The MFS is a large family of transporter capable of transporting small solutes in response to chemiosmotic ion gradients (Pao et al., 1998;

Walmsley et al., 1998). These MFS transporters contain a pair of monocarboxylate transporter (MCT) with 11-12 TMDs (Figure S2C). The MCTs play essential roles in the transport of nutrients, such as pyruvate, lactate, amino acids and so on, in the plasma membrane of human cells (Felmlee et al., 2020). These features attracted our intense attention, and thus named the MCTs as **A**picoplast **M**onocarboxylate **T**ransporters (AMTs, AMT1 for HAP3, TGGT1_233540; AMT2 for HAP4, TGGT1_297245).

We noticed that these two transporters are absent in red algae, green algae and plants (Figure 2B). This observation is in contrast to APT1, which was identifiable in these primary plastid-containing taxa (e.g. plants) but not in cyanobacteria (Figure 2B). Evolution and phylogenetic analyses suggested that the plant orthologues of APT1 are derived from a putative host cell that previously engulfed a cyanobacteria (Knappe et al., 2003; Weber et al., 2006). The pair of AMTs appears similar to the APT1 situation, indicating that they were possibly derived from the heterotrophic protist – the putative host cell - that previously engulfed a red alga. The AMTs were identifiable in the photosynthetic relative (e.g. *Chromera velia*) of the apicomplexans, and a distant relative taxa of Oomycetes (Figure 2A), indicating a broader conservation in these species. We further analyzed orthologues in selected species of apicomplexans, and found that most species contain at least two identifiable orthologues, including *Crytosporidium spp*. (Table S11). Collectively, the pair of AMTs are likely to have critical roles in metabolic integration of the endosymbiont in the parasite cytosol during evolution.

AMT1 and AMT2 are essential for the parasites

The confocal imaging showed that AMT1-6Ty was almost perfectly co-localized with AMT2-6HA (Figure S3A), suggesting that the putative transporters are highly likely to be localized at the apicoplast membranes. In support of this model, immuno-Electron Microscopy (immuno-EM) provided a further piece of evidence, supporting the membrane localization of AMT1 and AMT2 (Figure S3B). Due to the complexity of the apicoplast membranes, and heterogeneity of immunolabeling, the precise topology of AMT1 and AMT2 within the apicoplast membranes merits future investigation. To analyze the physiological functions of the AMTs, we generated the conditional knockdown lines using an IAA-inducible degron (AID) system in *T. gondii* (Brown et al., 2017; Long et al., 2017b). The CRISPR-Cas9 genome editing approach was utilized to specifically fuse the AID-6Ty at the 3'-terminus of the genes in the IAA receptor (TIR1) expressing line RH TIR1 (Figure S4A). To conditionally study both proteins together, we fused AMT2 with AID-3HA at the 3'-terminus in the background of AMT1-AID-6Ty, creating a double knockdown line AMT1-AID-6Ty/AMT2-AID-3HA (dKD). Correct integration of the AID fragments was confirmed by diagnostic PCR as demonstrated in the schematic diagram (Figure S4A-B). As expected, the AID fusions were efficiently and stably depleted in IAA treatments for 3-36 hours, as shown on Western blots (Figure 3A). It was noteworthy that Western blots detected two bands in the single and double AID fusion lines, which appeared to be the precursor and mature forms of AMT1 and AMT2 (Figure 3A). So far, several membrane proteins have been identified in the apicoplast of *T. gondii*, four of which were observed to be processed (FtsH1, TiC20, ATrx1 and TPC) (DeRocher et al., 2008; Karnataki et al., 2007; Karnataki et al., 2009; van Dooren et al., 2008). Yet, at least ATrx1 and FtsH1 lack canonical signal peptides. However, in *P. falciparum*, PfiTPT is processed and cleaved, while PfoTPT is unprocessed due to its absence of a signal peptide (Mullin et al., 2006). It appear that processing and topology of ATMs are complex and unpredictable in *T. gondii*. Further analysis by IFA showed that the AID fusions were correctly localized to the apicoplast and were depleted within 24 hours of IAA treatment (Figure 3B and Figure S4C); however, the parasite bodies were morphologically normal. To assess lytic growth of the AID lines, we assayed plaque formation of the AID parasites on host cell monolayers for 7 days. We observed that the AID lines grown in IAA did not form discernible plaques (Figure 3C),

which was supported by further analysis of the plaque numbers and areas (Figure 3D-E). In summary, the AMTs are potentially essential for *in vitro* parasite growth.
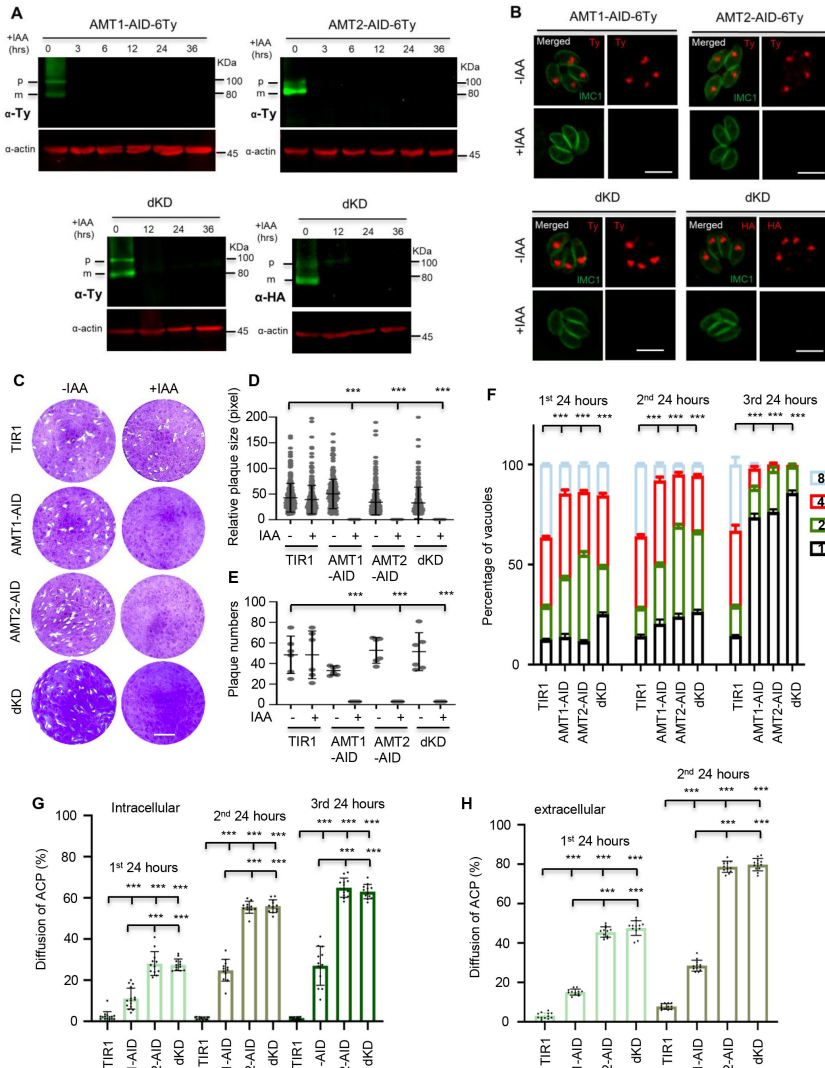

Figure 3.

AMT1 and AMT2 are localized at the apicoplast membrane and essential for parasite growth *in vitro*

(A) Western blot detection of protein depletion in the AID lines. The lines were induced by auxin (IAA) for different hours (hrs) as indicated. Western blots detected immatured (p) and matured (m) forms of the protein fusions in the non-induced lanes. Actin served as the control.

(B) IFA detection of protein depletion in the AID lines. Parasites were grown in IAA for 24 hours, followed by IFA with antibodies against Ty or HA (red) and IMC1 (green). Scale = 5 μm.

(C-E) Plaque formation by the TIR1 and AID lines on HFF monolayers in ± IAA for 7 days. Numbers (D) and sizes (E) of the plaques were measured by ImageJ. Scale = 0.5 cm. Two independent experiments with triplicates were performed. Data are shown as a mean ± SEM.

(F) Parasite replication of the TIR1 and AID lines grown in IAA. The parasites were grown in IAA for 24 hours, followed by scraping, harvesting and infection for the 2nd and 3rd rounds of parasite growth in IAA. The parasites stained with GFP45 were counted in vacuoles (at least 150 vacuoles in each replicate). In comparing to TIR1 (1st, 2nd and 3rd), *p*<0.0001 for the AID lines with 2 and 8 parasites/vacuole in the 1st round, and for the AID lines with 1-8 parasites/vacuole in the 2nd round, *p*<0.0001 for the AID lines with 1 and 4 parasites/vacuoles in the 3rd round.

(G-H) ACP diffusion in the TIR1 and AID lines grown in IAA. Parasites were grown in IAA for the 1st, 2nd and 3rd lytic cycles, as described in the parasite replication assay (intracellular parasites). Those parasites in the 1st and 2nd round of growth were forced to egress for the same analysis (extracellular parasites). Vacuoles or single parasites were scored (n>150 for each replicate).

Fields/images were selected blind and all parasites/vacuoles were scored on the same fields/images (F-H). Three independent experiments were performed (A, B, F, G and H), data are shown as a mean ± SEM with two-way ANOVA with Tukey's multiple comparisons (compared with the TIR1). ***, *p*<0.0001.

We wondered if parasite replication contributed to the plaque defects. The parasites were grown in IAA for 24 hours, followed by scraping, purification and re-infection for the assay in the 2nd 24 hours and 3rd 24 hours. Using IFA analysis of the parasites, we observed that parasite replication was significantly affected in the first 24 hours of growth and became worse in the following cycles of 24 hours, especially the 3rd 24 hour period (Figure 3F). These results suggested that depletion of the transporters caused strong growth defects and delayed death of the parasites. We wondered if depletion of the proteins could cause loss or breakdown of the apicoplast, as reported previously for many apicoplast proteins (Kennedy et al., 2019b). ACP, an apicoplast marker, was used to test the apicoplast status (Waller et al., 1998). We observed that ACP partially diffused in the cytosol of intracellular parasites grown in IAA for 24 hours (Figure S5A), whereas it completely diffused in the cytosol of extracellular parasites that had grown in IAA for 24 hours (Figure S5B). This observation suggested swelling or breakdown of the apicoplast in the intracellular or extracellular parasites depleted with the AMTs, respectively. Detailed analysis of the phenotypes showed that the ACP diffusion gradually increased while comparing the three cycles for the same AID line in both the intracellular and extracellular parasites (Figure 3G-H). However, it was as low as ~30% in AMT1-AID, compared to those (60-70%) in AMT2-AID and dKD (Figure 3G-H). These results suggested that depletion of AMT2-AID resulted in much more severe defects (swelling or breakdown) of the apicoplast than that of AMT1-AID, and further depletion of AMT1-AID had no further effect.

Depletion of the proteins resulted in defects in metabolic pathways

Based on the evolutionary predictions and features of monocarboxylate transporters, we suspected that the AMTs might be involved in transport of substrates, such as pyruvate, lactate, amino acids, as reported for human MCTs (Felmlee et al., 2020). As such, depletion of AMT1 and AMT2 would result in reduced levels of the metabolites of IPP and fatty acids in *T. gondii*. We first designed experiments to examine the possible defect of IPP synthesis in the AID lines upon induction, by assaying the capabilities of endocytic trafficking of GFP vesicles to the vacuolar compartment (VAC) (Dou et al., 2014). Our recent data showed that GFP transport to the VAC following its uptake from host cell cytosol is dependent on protein prenylation of Rab1B and YKT6.1 (unpublished data). These proteins are modified at the C-terminal motif by isoprenoids, the synthesis of which could be specifically inhibited by atorvastatin at the host cells and by zoledronate in the parasite (Li et al., 2013), as demonstrated in a schematic and in positive experiments (TIR1 with two drugs at IC50 concentrations) with reduced GFP transport (Figure 4A-B). Therefore, measuring the endocytic trafficking of GFP vesicles in parasites in the absence/presence of atorvastatin could reflect levels of protein prenylation, and thus levels of IPP synthesis in the parasites. We then assayed the TIR1 and AID lines by growing them in GFP expressing HFF monolayers, where experimental groups were controlled by absence/presence of atorvastatin and IAA (Figure 4B), and where LHVS was added to avoid degradation of GFP in the VAC. Following endocytosis of GFP vesicles by the micropore (manuscript in press), GFP vesicles were successfully transported to and accumulated in the VAC of TIR without IAA, with a high percentage (>20%) of parasites containing GFP foci (Figure 4B). In contrast, the GFP vesicles diffused through the cytosol, and were unable to accumulate at the VAC in the AID parasites grown in IAA with the absence/presence of atorvastatin, as shown by significantly reduced percentages (~8%) of the parasites in the AID lines induced for 12 hours (Figure 4B). We further tested Rab1B stability in the AMT-AID lines grown in IAA for 12 hours, which showed a strong defect of reduced protein abundance of Rab1B by scoring of parasites with normal or abnormal level of Rab1B using an IFA approach (Figure S5C). This phenotype was observed in parasites with a reduced supply of isoprenoids by drug

inhibition or knockdown of prenyl-transferase GGT-2 (unpublished data). These results altogether thus suggested that the IPP synthesis is significantly decreased in the AID lines depleted with the transporters. However, it was noteworthy that parasites depleted with AMT1-AID and AMT2-AID had similar levels of reduced GFP transport and parasites with reduced protein abundance of Rab1B at the 12 hours of IAA induction, suggesting that depletions of AMT1 and AMT2 resulted in similar levels of IPP reduction in parasites.

Figure 4.

Depletion of AMT1 and AMT2 caused defects of MEP and FASII pathways (A-C) The MEP activity was strongly affected in the AID lines. GFP transport to the VAC was assayed by growning parasties in GFP expressing HFF cells (HFF-GFP). LHVS (10 µM) was added to inhibit GFP digestion in the VAC (Dou et al., 2014). The isoprenoid synthesis in host cells and parasites was inhibited by IC50 concentrations of atorvastatin (10 µM) and zoledronate (0.3 µM)(Li et al., 2013), respectively (A). The inhibition over the TIR1 line using two of the drugs was used as a positive control (B). The AID parasites were grown in HFF-GFP cells in the presence of LHVS for 36 hours in total, with the addition of atorvastatin, zoledronate or IAA as stated for different experiments in the figure in the last 12 hours. Parasites were immediately harvested, adhered and scored, as shown in the example images in B. Percentages of parasites with GFP foci were plotted (C). Fields/images were selected blind and all parasites/vacuoles were scored on the same fields/images (C). Three independent experiments with triplicates were performed. Data are shown as a mean ± SEM with one-way ANOVA with Tukey's multiple comparison. ***, $p<0.0001$, scale = 5 µm.

(D-F) Fatty acid synthesis and TCA metabolites were significantly reduced in IAA induced AID parasites. Parasites were grown in IAA for 18 hours and harvested for untargeted metabolomics with GCMS and LCMS (N=3), and metabolites detected were analyzed by Dunnette's multiple comparison by comparing the AID parasites to the TIR1. Three AID lines shared 13 differential metabolites (D). These shared metabolites included fatty acids and lipids, such as myristic acid, palmitoleic acid, oleic acid, and phosphatidylcholine (PC) (E), and metabolites related to the TCA cycle (F). *, $p<0.05$; **, $p<0.001$; ***, $p<0.0001$.

Our results in *T. gondii* reported a physiological effect that was observed in *P. falciparum*, where inhibition of the MEP pathway by fosmidomycin caused disruption of hemoglobin transport (Howe et al., 2013; Kennedy et al., 2019a). Herein, our results underscored the importance of the transporters for supporting the MEP pathway in the apicoplast. This was further manifested by a reduced level of mitochondrial membrane potential detected by

mitotracker red in the AMT1-AID or AMT2-AID lines grown in IAA for 24 hours (Figure S5D). IPP is the precursor for synthesis of ubiquinone, an essential electron carrier required for electron transport in the mitochondria (Kennedy et al., 2019b; Sleda et al., 2022). The reduced mitochondrial potential was also observed in the parasites depleted with APT1 (Brooks et al., 2010). Thus, the reduced mitochondrial membrane potential provided another piece of evidence supporting the notion of defective IPP synthesis in parasites depleted with the transporters.

We further examined activity of the FASII pathway in the TIR1 and AID lines grown in IAA for 18 hours, by testing metabolites (e.g. FA) in the parasites using untargeted metabolomics (GCMS and LCMS). The metabolomics detected 66 metabolites in total in these lines (Dataset S2). After analyses using Dunnette's multiple comparison methods, 15, 23, and 34 differential metabolites were identified in the parasite groups depleted with either AMT1-AID, AMT2-AID or both (dKD) (Table S12), in comparison with TIR1. Interestingly, three AID lines shared 13 differential metabolites (Figure 4C). The shared metabolites included fatty acids and lipids, such as myristic acid (C14 fatty acid), palmitoleic acid (C16 fatty acid), trans-oleic acid (C18 fatty acid) and phospholipids containing C14 and C18 fatty acids (Figure 4D). These results were consistent with previous studies where inactivated FASII proteins led to reduced synthesis of fatty acids up to 18 carbons long, and exogenous additions of the C14 and C16 fatty acids could complement growth defects (Liang et al., 2020; Ramakrishnan et al., 2012). These results suggested that depletion of the transporters significantly impaired FASII activity. In contrast to the same level of reduced endocytic trafficking of GFP vesicles in the AID lines, reduction in levels of the C14, C16 and C18 fatty acids was much stronger and more significant in AMT2-AID and dKD than in AMT1-AID (Figure 4D), supporting the notion of a stronger impairment of the FASII pathway in parasites depleted with AMT2-AID.

Intriguingly, the metabolomics also identified metabolites related to the TCA cycle, such as gamma-aminobutyric acid (GABA), glutamic acid, and succinic acid (Figure 4E), which were shared among three of the AID lines. This would likely result from defective membrane potential caused by a reduced supply of IPP for synthesis of ubiquinone, as described above, or synthesis of heme that requires co-operation between the mitochondrion and the apicoplast (Harding et al., 2020). Another two metabolites, creatine and lactic acid, were likely associated with reduced metabolic levels in the parasites (Figure 4E).The untargeted metabolomics tends to identify differential metabolites by comparing the AID to TIR1 lines. Pyruvate was not identified, as it is actually a product of glycolysis in the cytosol. Collectively, the transporters are expectedly associated with the MEP and FASII pathways, to support synthesis of IPP and FA in the apicoplast.

Depletion of AMT2 affects stability of ACC1

Depletion of AMT2 resulted in stronger defects on ACP diffusion and synthesis of fatty acids, suggesting a more important role of AMT2 in the apicoplast. To find out the reason for this, we first examined the protein level of one AMT (fused with 6HA) in another AMT's AID-Ty line, thus assuring no reciprocal effect on protein level. After IAA induction for 36 hours, we did not see obvious changes to protein levels in the 6HA fusions in the AID-Ty lines on western blots and IFA (Figure S6A-B). Considering a MCT could transport biotin in mammalian cells (Daberkow et al., 2003), we wondered if AMT2 was able to transport biotin for activation of acetyl-CoA carboxylase ACC1, which is a key enzyme in FASII (Zuther et al., 1999). ACC1 was endogenously fused with 6HA in the AID lines by a CRISPR approach. Upon protein depletion in IAA for 36 hours, ACC1 was found to be gone only in the AMT2-AID parasites, but not in the AMT1-AID parasites, as demonstrated by Western blots (Figure S6C). Further analysis showed that ACC1 was gone in some parasites within a single vacuole in the AMT2-AID-depleted parasites, where ACP was clearly stained with a slight diffusion (Figure 6D). Based on the presence or absence of ACC1 in parasites of the vacuoles, we can classify

the vacuoles into three types - all parasites without ACC1 (type 1), one parasite (type 2) or two parasites (type 3) with ACC1 (Figure S6E). The quantification assay showed that only ~40% of the vacuoles contained one or two parasites with ACC1 signal (type 2 and type 3) (Figure S6F). However, ACC1 in those parasites was still biotinylated, as shown in streptavidin stains (Figure S6G). Collectively, AMT2 is associated with stability of ACC1 in a way, as yet, unknown, but unrelated with biotin availability in the apicoplast.

AMT2 is essential to parasite growth in mice

We next examined the *in vivo* growth of the AID parasites in mice administered with IAA. Prior to the mice assay, we attempted to gain further information about the ultra-structures of the apicoplast upon depletion of the AMTs. The transmission electron microscopy (TEM) demonstrated that the four membranes surrounding the apicoplast remained visible, but were loosened, and the interior of the organelle appeared less dense and even electron lucent in the AID parasites, which had been induced for 24 hours in comparison with the TIR1 parasites (Figure 5A). We further quantified the apicoplasts with a reduced electron density in the AID parasites induced for 12, 24 and 36 hours vs the TIR1 in IAA for 36 hours, by examining 300 parasites in each time point. This examination showed that the apicoplast numbers identified by TEM dropped in the AMT1-AID parasites, when induced for 24 hours and 36 hours, and the numbers dropped by much greater levels in the AMT2-AID parasites, following 12 hours of IAA induction (Figure 5B). Notably, the apicoplast was identified only 3 times in the AMT2-AID parasites at 36 hours induction. Accordingly, the percentage of the abnormal apicoplast increased for both of the AID lines. In contrast, depletion of AMT2-AID resulted in much higher levels of abnormal apicoplasts at the three induction time points, compared to those in parasites depleted with AMT1-AID (Figure 5B). These results suggested that depletion of AMT1 caused modest loss of the apicoplast, yet the AMT2 depletion appeared to have a greater effect on the apicoplast loss.


Figure 5.

Examination of the apicoplast ultra-structures, and mouse virulence of the parasites upon depletion of the AID fusions.

(A) Transmission electron microscopy (TEM) observed less electron dense or electron lucent lumen and loosened membranes in the apicoplast in the AID parasites induced in IAA for 24 hours. Representative images were shown. Scale = 200 nm.

(B) Quantification of the apicoplast with the lumen less dense or lucent in parasites induced for 12, 24 and 36 hours and TIR in IAA for 36 hours. The TEM examined 300 parasites for three lines (TIR1, AMT1-AID and AMT2-AID) at each time point, and numbers of abnormal apicoplast (red numbers) and apicoplast identified (green numbers) were shown by the columns. The columns express the percentages of
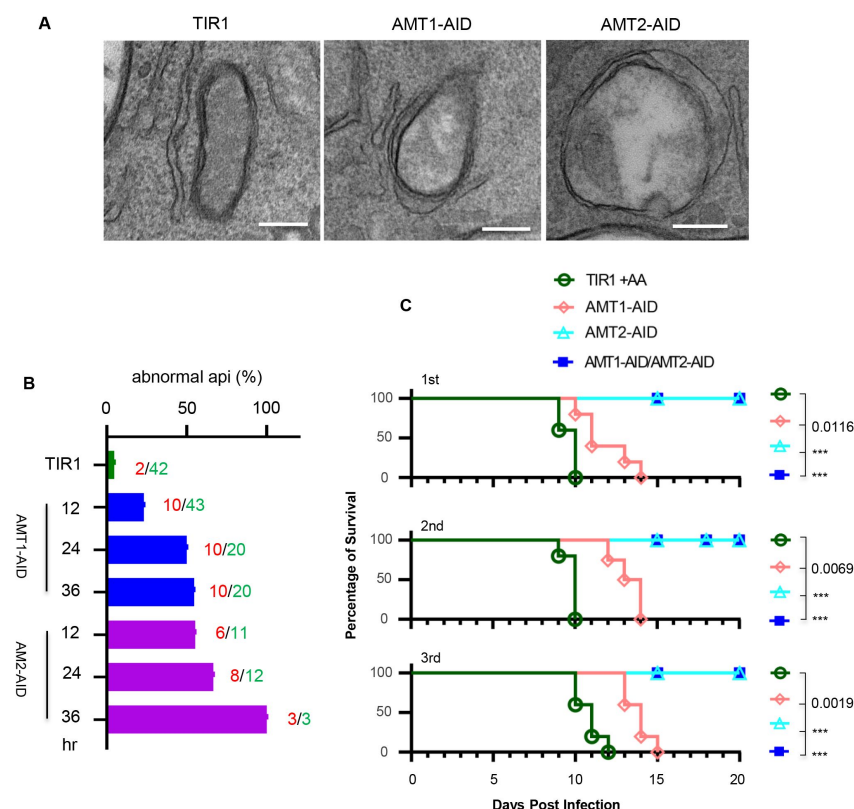
abnormal apicoplast in all the identified apicoplasts.

(C) Survival curve of BALB/C mice infected with 100 parasites intraperitoneally and treated with IAA for 20 days. The Gehan-Breslow-Wilcoxon test was used to compare differences between the survival curves (the AID line versus TIR1), ***, $p<0.0001$. The experiment of mouse infection was performed with 5 mice in each group, and results from three independent experiments (1st, 2nd and 3rd) were shown together with symbols for the mouse groups.

The parental line TIR1 and its derivative lines (AMT1-AID, AMT2-AID and dKD) were then used to intraperitoneally infect mice, at 100 parasites per mouse, followed by administering the mice orally and intraperitoneally with IAA in a solution on a daily basis. Those mice infected with TIR1 succumbed to lethal toxoplasmosis by day 10 post infection (Figure 5C). Conversely, the IAA treatment ultimately prevented acute virulence caused by the parasite lines with the AMT2 depletion (i.e. AMT2-AID and dKD), and it postponed mouse death by the AMT1-AID depletion. We next tested sera extracted from the surviving mice (which were infected by AMT2-AID) by performing IFA on *T. gondii* parasites. The IFA showed that the mouse sera clearly recognized proteins of the parasitophorous vacuoles of the parasites (Figure S7A). We also further analyzed the efficacy of protein degradation of the AMT1-AID fusions in mice, by treatment with or without IAA for 24 hours after 5 days of growth, as illustrated in Figure S7B. It was clear that AMT1-AID was efficiently degraded in mice by the treatment of IAA in only 24 hours (Figure S7B). These results demonstrated that the mice infection assays were robust. However, the strong growth conferred by AMT1 depletion in parasites in cell culture surprisingly resulted in only reduced parasite virulence in mice. We assume that this discrepancy is related to the relatively modest defects, such as the ACP diffusion/apicoplast abnormality (revealed by TEM)/FASII activity, as observed in the AMT1-depleted parasites. Thus, the remaining apicoplast is still functionally generating adequate amount of metabolites, allowing the parasites to survive in mice. However, the discrepancy is possibly associated with transport capability of substrates by AMT1 and AMT2. Though this does not perfectly explain the discrepancy, phenotypes in AMT1-depleted parasites argue for this possibility. Collectively, AMT2 was obviously essential for establishing *T. gondii* infection and growth in mice.

Discussion

Most of the apicomplexan parasites, such as *T. gondii* and *Plasmodium spp.*, harbor a vestigial plastid, which undergoes several fitness-conferring or essential metabolic pathways in the matrix (Kloehn et al., 2021; Lim and McFadden, 2010). However, the transporters that are responsible for exchanging metabolites between the apicoplast and the parasite remain elusive, due to difficulties in identification of those transporters in the multiple membranes that surround the organelle. Here we fully exploited the currently available data, and the high-efficiency of proximity biotin labeling and CRISPR-Cas9 tagging approaches in the model apicomplexan *T. gondii*, and discovered several novel transporters in the apicoplast. Among those putative transporters, most of them appear to be derived from the endosymbiont (i.e. a red alga) in evolution of the secondary plastid, and only the pair of monocarboxylate transporters AMT1 and AMT2 is likely to be derived from the putative host cell that originally engulfed the endosymbiont. Protein depletion of the AMT1 and AMT2, using a highly efficient technique the TIR1-AID system, resulted in defects of plaque formation *in vitro*, ACP diffusion/apicoplast loss, and biosynthetic pathways of the MEP and FASII. However, depletion of AMT2 clearly caused stronger defects including ACP diffusion/apicoplast loss, FASII products fatty acids, ACC1 stability and removed mouse

virulence. These results indicate that complex transporting functions are likely to exist in the apicoplast for AMT1 and AMT2.

Recent studies have highlighted the difficulty in identifying apicoplast transporters, because of strong backgrounds in the proteomics (Boucher et al., 2018; Sayers et al., 2018). This remained true for our proximity proteomics from APT1-TurboID. Fortunately, our focused screening leveraged high efficiency by genomic editing in *T. gondii,* yielding positive results for 12 putative transporters. These novel transporters provided an important resource for evolution and functional analyses. Their conservation, including in plastid-deficient taxa, i.e. Gregarina and Cryptosporidia, indicates that these proteins were relics of the former plastid in evolution via endosymbiont gene transfers (EGT) (Gould et al., 2008). Studies suggested that the metabolic integration of the primary plastid (e.g. chloroplast) was mainly driven by targeting transporters from a heterotrophic protist - the host cell, but not from the endosymbiont - cyanobacteria (Karkar et al., 2015; Tyra et al., 2007). However, our preliminary study in evolution indicated that most novel transporters were likely to be derived from the endosymbiont. In sharp contrast, the pair of monocarboxylate transporters (AMT1 and AMT2) may have an origin in a heterotrophic protist – the putative host cell. This observation therefore provides a perspective that the pair of AMTs may play critical roles in metabolic integration of the algal endosymbiont into the parasites.

Our immuno-EM and confocal imaging provided a strong support for the membrane localization of the pair of transporters AMT1 and AMT2 in the apicoplast, indicating that the AMTs are likely to transport substrates in the membranes. We observed that the AMTs are clearly processed, though they lack signal peptides. Concerning the processing and targeting, apicoplast membrane proteins in *T. gondii* appear to be more complex than those in *P. falciparum*, by comparison to PfiTPT and PfoTPT (Mullin et al., 2006). Our phenotypic analysis showed that depletion of the transporters AMT1 and AMT2 caused strong defects on plaque formation and parasite replication, suggesting that both transporters are critical on the apicoplast membranes. However, we observed disparate degrees of phenotypic disruption in the AMT1-depleted and AMT2-depleted parasites. Depletion of AMT2 always caused stronger defects in ACP diffusion, FASII fatty acids, apicoplast loss and mouse virulence. AMT2 is additionally associated with loss of ACC1, a key enzyme for FASII, found in the majority of parasites in a vacuole, likely providing another piece of evidence to explain the greater phenotypic defects. Several attempts to delete ACC1 failed in our study, supporting a critical role of ACC1 in the FASII process. Genetic studies suggest that depletion of FASII enzymes led to loss of apicoplast (Krishnan et al., 2020; Liang et al., 2020). Thus, the observation of ACC1 loss support stronger phenotypes in AMT2-AID depleted parasites. In addition, depletion of the AMTs caused an initially gradual defect, but then a much more focused sharper defect in parasite replication in the 3rd 24 hours and showed a delayed death phenotype. Previous studies showed that parasite replication exhibited gradual deceases upon depletion of TPC and APT1 by utilization of a low efficient knockdown strategy - the tetracyclin-inducible system (TATi) (Brooks et al., 2010; Li et al., 2021). It is unknown that the TATi system would mask the growth phenotype, yet, the AMT depletion appeared to have such a sharper change in the third cycle (24 hours in a growth cycle). Collectively, the AMTs are critical to parasites, yet AMT2 is more important to the apicoplast membrane function.

Based on knowledge of MCTs (Felmlee et al., 2020), the pair of AMTs is likely to transport pyruvate, lactate, amino acids and other substrates. We thus suspect that AMT1 and AMT2 might be associated with transporting pyruvate and amino acids, since these are essential for the apicoplast metabolism. Pyruvate is the central metabolite that connects many metabolic pathways in living organisms. It must be imported into organelles for specific metabolic pathways, as suggested with pyruvate import by the NHD1/Bass2-protein coupling function in the chloroplast of C4 plants, and by the mitochondrial pyruvate carrier MPC (Bricker et al., 2012; Furumoto, 2016; Furumoto et al., 2011; Gasperotti et al., 2020; Herzig et

al., 2012). In *T. gondii*, and *P. falciparum*, studies have suggested that the major pyruvate source has still not been established (Niu et al., 2022; Swift et al., 2020; Xia et al., 2019). The possible role on pyruvate import by the AMTs could provide a good explanation for the defects on MEP and FASII pathways, especially on the reduced levels of IPP synthesis resulting from the protein depletion. We attempted to define this possible function of the AMTs by a pyruvate sensor PyronicSF in the parasite (Arce-Molina et al., 2020), and by a complementation of an *Escherichia. coli* knockout strain that is deficient in pyruvate import (a generous gift from Prof. Kirsten Jung) (Gasperotti et al., 2020); however, several attempts with these approaches were not successful for detailed examination of pyruvate import capability either in the parasite or in the *E. coli* strain.

Our work successfully identifies several novel apicoplast transporters, thus greatly unravelling the mystery of the apicoplast membrane composition and opening up the possibilities to tackle difficult questions about metabolite transport in the apicomplexans. The most intriguingly findings in this study are the identification of the pair of monocarboxylate transporters AMT1 and AMT2, which are likely derived from the putative host cell that engulfed a red algal during the evolution of this group of parasites. Metabolic analysis together with other phenotypic analyses supported the notion that the pair of AMTs is associated with the MEP and FASII biosynthesis pathways. However, though both transporters belong to the MCTs, the phenotypic defects differ greatly, supporting a complex function for AMT2 in the apicoplast. Collectively, the monocarboxylate transporters are likely to control similar essential processes in related protists.

Limitations of This Study

This study has begun to look into the possibly evolutional origins of newly identified transporters although, as yet, observations are preliminary and await further analysis to clarify specific questions, as demonstrated in the detailed evolutionary analysis of chloroplast transporters (Karkar et al., 2015). Our further analysis on the phenotypes of two of these transporters, AMT1 and AMT2, using parasites depleted with these activities, demonstrates differing degrees of defects at critical points in the parasite's physiology and metabolism. We also observed similar decreases in level of the MEP biosynthesis activity upon depletion of AMT1 and AMT2, indicating that phenotypic outcomes did not result from apicoplast abnormality, since other phenotypic outcomes were more severe in the AMT2-depleted parasites. We predict, therefore, that the metabolic defects possibly result from a reduced supply of substrates by each of the transporter. It is noteworthy that other studies provided us comparable knowledge in phenotypes in TPC-depleted and APT1-depleted parasites. In these parasites, metabolic defects in the apicoplast pathways were observed by indirect measurements (Brooks et al., 2010; Li et al., 2021); however, these phenotypes were possibly caused by pleitropic effects of apicoplast loss, since they were analyzed by a comparably slow inactivation system to deplete the transporters of TPC and APT1 (with an induction of at least 3-4 days). Nevertheless, in our case with a highly efficient inactivation system, we still cannot exclude the effect of apicoplast loss on phenotypic results caused by depletion of the AMTs. Therefore, a more precise understanding of the functions of the AMTs will require further identification of the topology, protein interactions and substrate transport capability in the complex configuration of the apicoplast membranes. Our work, as yet, unsuccessful, in attempting to use a pyruvate sensor and/or a heterologous expression the AMTs in *E. coli,* is the first attempt to examine the transport capability of pyruvate by AMT1 and AMT2. Thereafter, application of more sophisticated approaches, such as *Xenopus* oocytes, an improved *E. coli* system, or a yeast expression system, may enable us to tackle the important question of substrate transport by AMT1 and AMT2. Future progresses on this

direction will thus shed critical insights into the discrepancies in parasite growth that we observe when comparing cell culture versus infections in mice.

Acknowledgements

Author Contributions

Conceptualization, S.L.; Methodology, H.D.; J.Y.; K.H.; W.B.Z.; J.L.; Investigation, H.D.; J.Y.; K.H.; W.B.Z.; H.Y.D.; R.B.W.; Formal Analysis, S.L.; H.D.; K.H.; J.Y.; D.H.L. Writing – Original Draft, S.L.; Writing – Review & Editing, S.L.; G.H.; K.M.B.; X.Q.Z.; D.H.L.;Z.R.L.; Funding Acquisition, X.Q.Z.; S.L.; D.H.L.; Resources, S.L.; D.H.L.; X.Q.Z.; Supervision, S.L..

Declaration of interests

The authors declare no competing interests.

Materials and Methods

Reagents and Antibodies

All chemicals were obtained from Sigma or ThermoFisher Scientific unless otherwise stated. Secondary antibodies used for immunofluorescence were conjugated to Alexa Fluor 488, Alexa Fluor 568, or Alexa Fluor 350 and were purchased from Invitrogen. Secondary antibodies used for western blots were IRDye 800CW or 680CW conjugates and were purchased from from LI-COR. Primary antibodies were listed as follows: rabbit anti-HA (Thermofisher, #71-5500), mouse anti-HA (BioLegend, #901501), mouse anti-C-myc (BioLegend, #626801), mouse anti-GFP (Thermofisher, #MA5-15349), mouse mAb 6D10 anti-MIC2 (Carruthers et al., 2000), rabbit anti-GRA7 (Alaganan et al., 2014) and mouse anti-Ty (BB2) antibodies. Antibodies, such as rabbit anti-ACP, rabbit anti-actin, mouse anti-IMC1, and rabbit anti-GAP45, were generated in our recent study (Wan et al., 2023).

Parasite and cell culture

T. gondii RHΔ*hxgprt*Δ*ku80* (Huynh and Carruthers, 2009), RHΔ*hxgprt*Δ*ku80*/TIR1 (Brown et al., 2017) and their derivative lines were listed in Table S2. The tachyzoite lines were grown in human foreskin fibroblast (HFF-1 from ATCC SCRC-1041) in D5 media prepared by DMEM supplemented with 5% inactivated fetal bovine serum (FBS) (Transgene, FS201-02), 10 mM glutamine and penicillin-streptomycin. The lines and HFF-1 were maintained mycoplasma negative as described previously (Long et al., 2016). The TIR1 and AID lines were cultured in HFF-1 with 500 μM auxin (+IAA) or 0.1% ethanol alone (-IAA) for phenotypic assays, as previously described (Brown et al., 2017; Long et al., 2017b). Parasites were harvested by passing through 22g needles and by filtration through 3.0 micron polycarbonate membranes, from which extracellular parasites were used for experimental assays.

Mice

T. gondii parasite growth *in vivo* was tested in six-week old BALB/C mice. Mice were maintained under specific pathogen-free (SPF) conditions in filter-top cages with provision of sterile water and food. Mice were randomly assigned to experimental groups (n=5 per group), and challenged by intraperitoneal (i.p.) injection of 100 *T. gondii* tachiyzoites, following by monitoring on a daily basis to record their health by checking their appearance, bodyweight and responsiveness. The mouse experiments were conducted according to the guidelines and regulations issued by the Veterinary Office of the China Agricultural University (Issue No. AW11402202-2-1).

Generation of Plasmids and *T. gondii* Lines

A CRISPR/Cas9 sgRNA 3' plasmid (Table S3) targeting a region close to a stop codon at a specific gene can efficiently produce Cas9 and sgRNA to create DNA double strand breaks (DSB) in parasites, which facilitates the integration of a tagging amplicon at the 3' terminus of a specific gene. The sgRNA specific sequences were selected, as described in our previous protocol (Brown et al., 2018). The sequences were integrated into the pCas9 plasmid using a basic seamless cloning and assembly kit (CU201-02, TransGen Biotech) with primers listed in Table S4, as described in our recent study (manuscript in press). The amplicon for a specific integration at the DSB was generated from a generic tagging plasmid (Table S3) using a pair of primers L and T (Table S4), as described in our previous study (Long et al., 2017b), which was illustrated in Fig. S$A. These generic plasmids included pL-6Ty-HXGPRT (Brown and Sibley, 2018), pL-6HA-DHFR (Long et al., 2017a), pL-6HA-HXGPRT (addgene #86552) (Long et al., 2017b), pL-TurboID-4Ty-DHFR (manuscript in press), pL-AID-6Ty-DHFR (manuscript in press) and pL-AID-3HA-HXGPRT (addgene #86553) (Long et al., 2017b). One additional generic plasmid pL-AID-GFP-HXGPRT was generated using pL-AID-3HA-HXGPRT as the PCR template of plasmid backbone, followed by cloning the GFP fragment into the backbone with primers listed in Table S4. The amplicon generated by primers L and T from the generic plasmids contains short homologs (HR1 and HR2, 41 bp) for targeting the upstream (HR1) of the stop codon and the downstream (HR2) of the Cas9 cleavage site (DSB), resulting in integration of epitope tags or AID fragments in frame with the encoding sequences of specific genes. The drug-selected lines were sub-cloned, followed with screening with diagnostic PCR, IFA and western blots. The resistance markers containing LoxP sites can be excised by transfection with pmini-Cre, as previously described (Heaslip et al., 2010).

Transfection and Selection

Parasites were harvested and resuspended in Cytomix (10 mM KPO$_4$, 120 mM KCl, 5 mM MgCl$_2$, 25 mM HEPES, 2 mM EDTA) 1x10^8 parasites/ml, then combined with 10-20 µg pCas9-sgRNA 3' and 1-5 µg amplicons with 2 mM ATP, 2 mM GSH and 150 µM CaCl$_2$ to a final volume of 250 µl, followed with electroporation using a BTX ECM 830 electroporator (Harvard Apparatus), as described previously (Soldati and Boothroyd, 1993). Parasites were selected on the second day with addition of appropriate drugs mycophenolic acid (MPA) (25 µg/ml) and 6-xanthine (6Xa) (50 µg/ml), or pyrimethamine (Pyr) (3 µM). Negative selection was applied with 6-thio-xanthine (200 µg/ml) when parasites were transfected with a pCre plasmid to remove the resistant marker HXGPRT. Positive selection pools of parasites were subcloned in 96-well plates at 3 parasites/well, and allowed to grow for 6-7 days before selection of wells containing a single plaque. Pure clones were diagnosed by PCR using appropriate primers (Table S4) and IFA analysis using appropriate antibodies if applicable.

Indirect Fluorescence Assay (IFA)

Parasites were fixed by 4% paraformaldehyde in PBS, followed by blocking and permeabilization using PBS containing 2.5% BSA and 0.25% Triton X100. Antibody incubation was performed with indicated combinations of primary antibodies for 30 min, followed by incubation with secondary antibodies conjugated with fluorescent dyes (Thermofisher Scientific) for 30 min. The above procedures were applied to the ACP diffusion analysis for parasites as stated in the results and legends. The blind counting was conducted for at least 150 vacuoles (intracellular parasites) or single parasites (extracellular parasites) in each replicate. ProLong Gold Antifade Mountant with or without DAPI were used to mount the coverslips on glass slides. Parasites were then imaged using a Nikon Ni-E microscope C2+ equipped with a DS-Ri2 Microscope Camera. The co-localization analyses were performed using the Ni-E software system NIS Elements AR. All the IFA analyses were carefully repeated at least three times, and similar results were obtained for the same experiments before finalizing the analysis.

Western blotting

Parasites were resuspended in PBS, followed by addition of 5x Laemmli sample buffer supplemented with 1 mM DTT for a further incubation at 98 °C for 10 min. Protein lysis was then resolved in SDS-PAGE, blotted by a BioRad wet-blotting system, subsequently incubated with different combinations of primary and secondary antibodies, followed by secondary antibodies conjugated with LI-COR reagents, or streptavidin LI-COR 800CW.. The blot membranes were then visualized by a Bio-RAD ChemiDOC MP system.

TurboID and Biotinylated Proteins

The APT1-TurboID line was grown on HFF monolayers for 24 hours, subsequently incubated with 500 µM D-biotin for 90 min. The parasites were fixed with 4% paraformaldehyde solution for IFA or harvested for western blots. IFA and western blots were performed with appropriate streptavidin reagents to visualize biotinylated proteins in parasites. The parental line and APT1-TurboID line were grown in HFF cells for 36 hours, followed with labeling of proteins by 500 µM D-biotin for 90 min, and harvesting of the parasites for purification of biotinylated proteins. In parallel, the APT1-TurboID parasites after 36 hours growing were harvested, and extracellular parasites were incubated with 500 µM D-biotin for 90 min, followed with by collection of parasites for purification of biotinylated proteins. The parasites were lysed in a buffer containing 1% Triton X-100, 0.2% SDS and 0.5%

deoxycholate, and sonicated with a microtip in 550 sonic dismembrator (ThermoFisher Scientific). Biotinylated proteins in cleared supernatant were purified using streptavidin magnetic beads, exactly following the protocol described elsewhere (Long et al., 2018).

Proteomic analysis

The purified proteins were separated on SDS-PAGE and stained by Coomassie blue R250, 45% methanol and 10% glacial acetic acid, subsequently dried on SDS-PAGE slices by vacuum. The dried gels were rehydrated, alkylated and washed to remove the stain and SDS, and subjected to steps of mass-spectrometry analysis, following the protocol described in the Bio-Protocol (Long et al., 2018). The parental line and TurboID fusion line were analyzed in parallel with three technical and biological replicates. Resulting spectra were searched against a combined database of *T. gondii* ME49 (http://ToxoDB.org, release 29) and human proteins and a decoy database, using Mascot and Scaffold. The current views in Scaffold were exported into an excel spreadsheet using the following settings of peptide 2, protein threshold 99% and peptide threshold 95%. Hits were analyzed using embedded tools in ToxoDB (https://toxodb.org/toxo/app/) to predict the transmembrane domain. Peptide numbers of the hits in the TurboID were compared to those in the parental line (0 peptide was considered as 1), and fold changes were used to plot a volcano map against $\text{Log10}^{p\ value}$ in ggplot2 package in R.

Conservation and phylogenetic analysis

The apicoplast proteins identified in this study and known apicoplast proteins as listed in the results (Table S10) were used as queries for searching orthologues in organisms in Eukaryote, including species belonging to the chromalveolates, plants, metazoan and fungi, and Bacteria (Table S9). These proteins were simultaneously searched with the profile Hidden Markov models (HMMs) search engine (jackhammer). The E-value cutoff was set at 1e-7 and hits with an E-value < 1e-7 were considered as orthologues. The best hits from the representative species in above taxa were merged and resultant list of orthologues (Table S10) were used for conservation analysis with ComplexHeatmap package in R (v4.2.0) (Gu et al., 2016). This analysis pulled up the protein conservation heatmap, with indication by a heat scaled with E-value for each individual orthologue. The tree dendrogram without meaningful branch lengths across these species, and across the proteins were clustered according to the Euclidean distance using UPGMA method. Representatives from the known apicoplast proteins were analyzed in parallel as the control for comparison.

Plaque Formation

Parasites (150 parasites) were inoculated on confluent HFF monolayers in one 6-well in plates, followed with addition of either 500 μM IAA or ethanol alone (0.1%) and growth in D5 media at 37°C for 7 days. The parasites and monolayers were then fixed with 70% ethanol for 15 min, stained with 0.5% crystal violet for 5 min, subsequently washed with dH2O and dried at room temperature. The plaque monolayers were recorded by scanning using a HP Scanjet G4050, and plaque numbers and plaque sizes were measured in ImageJ.

Parasite Replication

The TIR1 and its derived AID lines were grown in 500 μM IAA for 24 hours on monolayers in 24-well plates with coverslips. The parasites were fixed with 4% paraformaldehyde for 10 min, followed with blocking and permeabilization with 0.25% Triton X-100 in PBS containing 2.5% BSA. The parasites were then incubated with GAP45 antibodies and secondary anti-

rabbit antibodies conjugated with Alexa Fluor 568. The coverslips were mounted and visualized under a Nikon Ni-E microscope C+. Vacuoles containing different numbers of parasites were scored on the same images with blindness, and at least 150 vacuoles were counted in each replicate of three independent experiments. Ratios of vacuoles containing different numbers of parasites were plotted against the total vacuoles examined.

GFP acquisition assay

HFF cells expressing cytosolic GFP were prepared in our previous study (manuscript in press). In brief, pLVX-EF1a-GFP-IRES-puromycin was combined with packaging plasmids psPAX2 (addgene #12260) and pMD2.G (addgene #12259) in Opti-MEM I (31985062, Gibco), and mixed with Fugene HD (E2311, Promega), and transfected into 293T cells. Viruses were collected and mixed with polybrene in a 12-well plate well containing 30-50% confluent HFF-1 cell monolayers. After 24 hours of post-transduction, the cell monolayers were re-seeded with incubation of puromycin (2.5 µg/ml) for 3 days. The cell monolayers were then maintained and expanded in D5 media. The TIR1 and AID lines were grown in the cell monolayers with IAA, 10 µM LHVS and 12.5 µM atorvastatin for 12, 24 or 36 hours. LHVS inhibits cysteine protease CPL to accumulate GFP derived from host cell cytosol, as reported previously (Dou et al., 2014), Atorvastatin can inhibit synthesis of FPP and GGPP in host cells, to decrease the supply of FPP and GGPP from the host cells to the parasites. In parallel, TIR1 was grown in the host cells with 10 µM LHVS, 0.3 µM zoledronic acid and 12.5 µM atorvastatin, serving as a positive control to observe defects in GFP transport by decreasing protein prenylation in parasites. The addition of atorvastatin and zoledronic acid could specifically inhibit the FPP and GGPP supply both in host cells and parasites (Li et al., 2013), thus inhibiting GFP transport to the VAC in parasites, as demonstrated in Fig. 5A-B. Purified parasites were adhered onto poly-lysine-coated coverslips, followed with fixation with 4% paraformaldehyde for 10 min. The parasites were permeabilized by 0.25% Triton X-100 in PBS, subsequently mounted in ProLong Gold Antifade Mountant with DAPI for visualization under a Nikon Ni-E microscope C+. Parasites were judged by observations of parasites with either GFP foci, GFP diffusion or GFP absence, as demonstrated in Figure 4B. Fields/images were selected blind, and all parasites in the same images were counted for scoring of parasites with or without GFP signal. The counting was performed in replicate for at least 150 parasites. Percentages of parasites containing GFP foci were calculated and expressed as percentages in the populations.

Immuno-staining for Electron Microscopy (Immuno-EM)

Parasites were grown on HFF monolayers for 24 hours, subsequently digested with trypsin for collecting samples. Samples were fixed in a 0.1 M sodium cacodylate buffer (pH7.4) containing 3% (w/v) paraformaldehyde, 0.1% glutaraldehyde (v/v), 4% sucrose (w/v) at 4°C overnight. The samples were then washed four times by a 0.1 M sodium cacodylate buffer containing 4% (w/v) sucrose, and neutralized on ice by a 0.1 M sodium cacodylate buffer containing 4% (w/v) sucrose, 0.1 M glycine, and dehydrated in ethanol. The samples were immersed in LR White resin (Ted Pella, Inc.) at 4°C overnight, subsequently polymerised at light intensity 1.2×10^5 µJ/cm^2 on ice for 5 hours. The LR White imbedded samples were sectioned with a Leica ultramicrotome (EM UC7) at 100 nm and were picked onto 100-mesh formvar-carbon-coated nickel grids. The loaded nickel grids were then blocked and incubated with mouse anti-Ty antibodies (1:5) at RT for 2 hours and overnight at 4°C, followed with washing by PBS. The samples on grids were incubated with Alexa FluorTM 488 goat anti-mouse IgG 10 nm colloidal gold particle (1:100) (15nm or 10 nm in size) for 1 hours, followed with washs in PBS and double-distilled water. The samples on grids were stained by 3% phosphotungstic acid and observed under a JEM1400FLASH transmission electron microscope operation at 120 KV.

Transmission Electron Microscopy (TEM)

Parasites grown on HFF cell monolayers were collected by scraping off, fixed by a fixative mixture of 2% paraformaldehyde and 3% glutaraldehyde at 4 °C overnight. The samples were washed, fixed in 1% osmium tetroxide in 50 mM phosphate buffer at 4 °C for 1 hour, washed three times and dehydrated by sequential concentration of ethanol, and by acetone and Spurr for 1 hour. The samples were then imbedded in Spurr and sectioned to 100 nm slices by a Leica ultrmicrotome (EM UC7). The ultrathin-sections were collected on 100 mesh grids. The grids were then viewed by JEOL transmission electron microscopy (JEM1400FLASH).

Untargeted Metabolomics

Parasites were grown in IAA for 18 hours and purified in chilled PBS, followed by immediate quenching by addition of -40°C methanol and sterile ddH2O (400 μl methanol + 100 μl H_2O). The samples were processed for the analysis of metabolites by GC-MS and LC-MS, exactly following the protocol reported in our recent study (manuscript in press). Briefly, the GC-MS analysis was performed with An OPTIMA 5 MS Accent fused-silica capillary column on Agilent7890A/5975C GC-MS system (Agilent Technologies Inc., CA, USA), while the LC-MS analysis was performed on a ThermoFisher Ultimate 3000 UHPLC system with a Waters ACQUITY UPLC BEH C18 column (2.1mm × 100 mm, 1.7μm) using standard positive and negative modes. For GC-MS, the peak picking, alignment, deconvolution and further processing of resulting raw data were carried out according to the previously published protocols (Gao et al., 2010). The final data was exported as a peak table file, including observations, variables (rt_mz), and peak areas. The data was normalized against the total peak value of total peaks, and differential metabolites were identified by statistical analysis performed in R platform, where parametric and nonparametric tests were done using One-way ANOVA with Dunnett's multiple comparison, to identify differential metabolites with $p<0.05$ and fold change >1.2 for further analysis. For LC-MS, The raw data was transformed to mzXML format by ProteoWizard and then processed by XCMS and CAMERA packages in R software platform. The final data was exported as a peak table file, including sample names, variables (rt_mz) and peak areas. The peak areas data was normalized to internal standards before the analysis of statistics. The in-house database was referenced to identify the compound by using m/z (MS1), mass spectra (MS2) and retention times (RT). Normalization for relative parasite amounts was based on the total integrated peak area values of metabolites within an experimental batch. Metabolites identified by the GCMS and LCMS were merged together for further analysis (Dataset S2). Enrichment of Metabolic Pathways (Table S13) were analyzed using the differential metabolites identified in three of the AID lines versus the TIR1 line. MetaboAnalyst 5.0 server was used to enrich the metabolite sets with KEGG, in which the p-value below 0.05 was considered to be significant.

Parasite growth in mice

Mice were randomly assigned to groups and were intraperitoneally injected with 100 parasites per mouse. Subsequently, mice (n=5 mice for each line) were orally administered with IAA (3-indoleacetic acid, auxin, Sigma) and by an intraperitoneal injection on a daily basis (Brown and Sibley, 2018; Yesbolatova et al., 2020). The drinking water contained sterile water with 1 mg/ml IAA, 3 mM NaOH, 5% sucrose (w/v), flavored with 2 mg/ml TANG (Mondelēz International), pH8.0. Meanwhile, mice were intraperitoneally injected with a daily 0.2 ml of sterile solution containing 15 mg/ml IAA, 1 M NaOH, pH7.8. The mice infected with the TIR1 line served as the control, which received the drinking water and injection of

IAA-containing solution in the same way to the AID lines. The mice were weighted and their health conditions were monitored on a daily basis until day 20.

Quantification and statistical analysis

Experiments were conducted blind for at least two-three biological replicates and statistical analyses were conducted in Graphpad v8.0. One-way or two-way ANOVA with Tukey's multiple comparison was conducted for data that fit normal a distribution or the Mann-Whitney test for non-parametric comparison, while one-way ANOVA with Dunnett's multiple comparison was tested for data with small sizes or abnormal distributions. $p<0.05$ was considered significant. Experiment-specific statistical information is provided in the figure legends or associated method details including replicates (n), trials (N), and statistical tests performed.

Data availability

The proteomic data reported in this paper have been deposited in the OMIX, China National Center for Bioinformation/Beijing Institute of Genomics, Chinese Academy of Sciences (https://ngdc.cncb.ac.cn/omix) with accession number: WgSMCBqN. The metabolomics raw data have been deposited in the MetaboLights (https://www.ebi.ac.uk/metabolights/) with accession number: MTBLS7060. Minimally processed data of the proteomics and metabolomics data are available in Dataset S1 and Dataset S2, respectively. *Toxoplasma gondii* genome information can be found in ToxoDB release 53 (http://toxodb.org) and Eukaryotic pathogen, Vector & Host Information Resources can be found in VEupathDB (http://veupathdb.org).

Legends for Dataset S1-S2 and Table S5-12

Dataset S1. Minimally processed mass spectrometry datasets of the APT1-TurboID fusion line and the parental line.

Dataset S2. Minimally processed datasets of untargeted metabolites detected by GCMS and LCMS in TIR1, AMT1-AID, AMT2-AID and dKD lines grown in IAA for 18 hours.

Table S5. Volcano analysis of mass-spectrometry datasets from APT1-TurboID and the parental line. Intracellular and extracellular parasites of APT1-TurboID were incubated with 500 µM biotin for 1 hours, and biotinylated proteins were purified for Mass spectrometry analysis together with the control line RH. Datasets were analyzed by student t test and plotted by Volcano analysis.

Table S6. List of known apicoplast proteins on the volcano plotting. The known proteins were listed with referenced PMID.

Table S7. List of TMD proteins identified by APT1-TurboID and ordered from high numbers to low numbers. The MS hits identified from APT1-TurboID were analyzed in ToxoDB for identification of transmembrane domains (TMD).

Table S8. Merged candidate list from three datasets of hyperLOPIT, ACP-BirA and APT1-TurboID. Candidates were retrieved from three datasets, and analyzed with their TMD numbers. Most listed proteins are putative transporters or proteins with high numbers of TMD.

Table S9. Proteins identified to be in the apicoplast by epitope fusion and confocal imaging. These newly identified apicoplast proteins were listed with CRISPR scores, TMD numbers, predicted localization by HyperLOPIT, and their P. falciparum orthologues with relevant information.

Table S10. Identification of orthologues of novel apicoplast proteins and known proteins in species belong to the chromalveolates, red algae, green algae, plants, fungi, metazoa and bacteria. The species were grouped into the taxa, and listed with their orthologues and E-values of the newly identified proteins.

Table S11. Orthologues of AMT1 and AMT2 in selected species of apicomplexans. Orthologous were analyzed in HMMER, and accession numbers of these orthologues in the apicomplexans were listed.

Table S12. Analysis of metabolites detected by GCMS and LCMS in the lines of TIR1, AMT1-AID, AMT2-AID and dKD induced by IAA for 18 hours. The datasets (Dataset S2) were analyzed by Dunnett's multiple comparisons.

References

1. Alaganan A. , Fentress S.J. , Tang K. , Wang Q. , Sibley L.D (2014) **Toxoplasma GRA7 effector increases turnover of immunity-related GTPases and contributes to acute virulence in the mouse** *Proc Natl Acad Sci U S A* **111**:1126–1131

2. Arce-Molina R. , Cortes-Molina F. , Sandoval P.Y. , Galaz A. , Alegria K. , Schirmeier S. , Barros L.F. , San Martin A (2020) **A highly responsive pyruvate sensor reveals pathway-regulatory role of the mitochondrial pyruvate carrier MPC** *Elife* **9**

3. Barylyuk K. , Koreny L. , Ke H. , Butterworth S. , Crook O.M. , Lassadi I. , Gupta V. , Tromer E. , Mourier T. , Stevens T.J. , et al. (2020) **A Comprehensive Subcellular Atlas of the Toxoplasma Proteome via hyperLOPIT Provides Spatial Context for Protein Functions** *Cell Host Microbe* **28**:752–766

4. Boucher M.J. , Ghosh S. , Zhang L. , Lal A. , Jang S.W. , Ju A. , Zhang S. , Wang X. , Ralph S.A. , Zou J. , et al. (2018) **Integrative proteomics and bioinformatic prediction enable a high-confidence apicoplast proteome in malaria parasites** *PLoS Biol* **16**

5. Branon T.C. , Bosch J.A. , Sanchez A.D. , Udeshi N.D. , Svinkina T. , Carr S.A. , Feldman J.L. , Perrimon N. , Ting A.Y (2018) **Efficient proximity labeling in living cells and organisms with TurboID** *Nat Biotechnol* **36**:880–887

6. Bricker D.K. , Taylor E.B. , Schell J.C. , Orsak T. , Boutron A. , Chen Y.C. , Cox J.E. , Cardon C.M. , Van Vranken J.G. , Dephoure N. , et al. (2012) **A mitochondrial pyruvate carrier required for pyruvate uptake in yeast, Drosophila, and humans** *Science* **337**:96–100

7. Brooks C.F. , Johnsen H. , van Dooren G.G. , Muthalagi M. , Lin S.S. , Bohne W. , Fischer K. , Striepen B. (2010) **The toxoplasma apicoplast phosphate translocator links cytosolic and apicoplast metabolism and is essential for parasite survival** *Cell Host Microbe* **7**:62–73

8. Brown K.M. , Long S. , Sibley L.D (2017) **Plasma Membrane Association by N-Acylation Governs PKG Function in Toxoplasma gondii** *mBio* **8**

9. Brown K.M. , Long S. , Sibley L.D (2018) **Conditional Knockdown of Proteins Using Auxin-inducible Degron (AID) Fusions in Toxoplasma gondii** *Bio Protoc* **8**

10. Brown K.M. , Sibley L.D (2018) **Essential cGMP Signaling in Toxoplasma Is Initiated by a Hybrid P-Type ATPase-Guanylate Cyclase** *Cell Host Microbe* **24**:804–816

11. Carruthers V.B. , Sherman G.D. , Sibley L.D (2000) **The Toxoplasma adhesive protein MIC2 is proteolytically processed at multiple sites by two parasite-derived proteases** *J Biol Chem* **275**:14346–14353

12. Cavalier-Smith T (1999) **Principles of protein and lipid targeting in secondary symbiogenesis: euglenoid, dinoflagellate, and sporozoan plastid origins and the eukaryote family tree** *J Eukaryot Microbiol* **46**:347–366

13. Cavalier-Smith T (2000) **Membrane heredity and early chloroplast evolution** *Trends Plant Sci* **5**:174–182

14. Daberkow R.L. , White B.R. , Cederberg R.A. , Griffin J.B. , Zempleni J (2003) **Monocarboxylate transporter 1 mediates biotin uptake in human peripheral blood mononuclear cells** *J Nutr* **133**:2703–2706

15. DeRocher A.E. , Coppens I. , Karnataki A. , Gilbert L.A. , Rome M.E. , Feagin J.E. , Bradley P.J. , Parsons M (2008) **A thioredoxin family protein of the apicoplast periphery identifies abundant candidate transport vesicles in Toxoplasma gondii** *Eukaryot Cell* **7**:1518–1529

16. Dou Z. , McGovern O.L. , Di Cristina M. , Carruthers V.B. (2014) **Toxoplasma gondii ingests and digests host cytosolic proteins** *mBio* **5**:e01188–1114

17. Fata J.J. , Rabuzzi D.D (1988) **Aggressive juvenile fibromatosis presenting as a parotid mass** *Ear Nose Throat J* **67**:681–672

18. Felmlee M.A. , Jones R.S. , Rodriguez-Cruz V. , Follman K.E. , Morris M.E (2020) **Monocarboxylate Transporters (SLC16): Function, Regulation, and Role in Health and Disease** *Pharmacol Rev* **72**:466–485

19. Fleige T. , Fischer K. , Ferguson D.J. , Gross U. , Bohne W (2007) **Carbohydrate metabolism in the Toxoplasma gondii apicoplast: localization of three glycolytic isoenzymes, the single pyruvate dehydrogenase complex, and a plastid phosphate translocator** *Eukaryot Cell* **6**:984–996

20. Foth B.J. , Ralph S.A. , Tonkin C.J. , Struck N.S. , Fraunholz M. , Roos D.S. , Cowman A.F. , McFadden G.I (2003) **Dissecting apicoplast targeting in the malaria parasite Plasmodium falciparum** *Science* **299**:705–708

21. Furumoto T (2016) **Pyruvate transport systems in organelles: future directions in C4 biology research** *Curr Opin Plant Biol* **31**:143–148

22. Furumoto T. , Yamaguchi T. , Ohshima-Ichie Y. , Nakamura M. , Tsuchida-Iwata Y. , Shimamura M. , Ohnishi J. , Hata S. , Gowik U. , Westhoff P. , et al. (2011) **A plastidial sodium-dependent pyruvate transporter** *Nature* **476**:472–475

23. Gao X. , Pujos-Guillot E. , Sebedio J.L (2010) **Development of a quantitative metabolomic approach to study clinical human fecal water metabolome based on trimethylsilylation derivatization and GC/MS analysis** *Anal Chem* **82**:6447–6456

24. Gasperotti A. , Going S. , Fajardo-Ruiz E. , Forne I. , Jung K (2020) **Function and Regulation of the Pyruvate Transporter CstA in Escherichia coli** *Int J Mol Sci* **21**

25. Gould S.B. , Waller R.F. , McFadden G.I. (2008) **Plastid evolution** *Annu Rev Plant Biol* **59**:491–517

26. Gu Z. , Eils R. , Schlesner M (2016) **Complex heatmaps reveal patterns and correlations in multidimensional genomic data** *Bioinformatics* **32**:2847–2849

27. Harding C.R. , Sidik S.M. , Petrova B. , Gnadig N.F. , Okombo J. , Herneisen A.L. , Ward K.E. , Markus B.M. , Boydston E.A. , Fidock D.A. , et al. (2020) **Genetic screens reveal a central role for heme metabolism in artemisinin susceptibility** *Nat Commun* **11**

28. Heaslip A.T. , Dzierszinski F. , Stein B. , Hu K (2010) **TgMORN1 is a key organizer for the basal complex of Toxoplasma gondii** *PLoS Pathog* **6**

29. Herzig S. , Raemy E. , Montessuit S. , Veuthey J.L. , Zamboni N. , Westermann B. , Kunji E.R. , Martinou J.C (2012) **Identification and functional expression of the mitochondrial pyruvate carrier** *Science* **337**:93–96

30. Howe R. , Kelly M. , Jimah J. , Hodge D. , Odom A.R (2013) **Isoprenoid biosynthesis inhibition disrupts Rab5 localization and food vacuolar integrity in Plasmodium falciparum** *Eukaryot Cell* **12**:215–223

31. Huynh M.H. , Carruthers V.B (2009) **Tagging of endogenous genes in a Toxoplasma gondii strain lacking Ku80** *Eukaryot Cell* **8**:530–539

32. Janouskovec J. , Horak A. , Obornik M. , Lukes J. , Keeling P.J (2010) **A common red algal origin of the apicomplexan, dinoflagellate, and heterokont plastids** *Proc Natl Acad Sci U S A* **107**:10949–10954

33. Karkar S. , Facchinelli F. , Price D.C. , Weber A.P. , Bhattacharya D (2015) **Metabolic connectivity as a driver of host and endosymbiont integration** *Proc Natl Acad Sci U S A* **112**:10208–10215

34. Karnataki A. , Derocher A. , Coppens I. , Nash C. , Feagin J.E. , Parsons M (2007) **Cell cycle-regulated vesicular trafficking of Toxoplasma APT1, a protein localized to multiple apicoplast membranes** *Mol Microbiol* **63**:1653–1668

35. Karnataki A. , DeRocher A.E. , Feagin J.E. , Parsons M (2009) **Sequential processing of the Toxoplasma apicoplast membrane protein FtsH1 in topologically distinct domains during intracellular trafficking** *Mol Biochem Parasitol* **166**:126–133

36. Kennedy K. , Cobbold S.A. , Hanssen E. , Birnbaum J. , Spillman N.J. , McHugh E. , Brown H. , Tilley L. , Spielmann T. , McConville M.J. , et al. (2019) **Delayed death in the malaria parasite Plasmodium falciparum is caused by disruption of prenylation-dependent intracellular trafficking** *PLoS Biol* **17**

37. Kennedy K. , Crisafulli E.M. , Ralph S.A (2019) **Delayed Death by Plastid Inhibition in Apicomplexan Parasites** *Trends Parasitol* **35**:747–759

38. Kloehn J. , Lacour C.E. , Soldati-Favre D (2021) **The metabolic pathways and transporters of the plastid organelle in Apicomplexa** *Curr Opin Microbiol* **63**:250–258

39. Knappe S. , Flugge U.I. , Fischer K (2003) **Analysis of the plastidic phosphate translocator gene family in Arabidopsis and identification of new phosphate translocator-homologous transporters, classified by their putative substrate-binding site** *Plant Physiol* **131**:1178–1190

40. Krishnan A. , Kloehn J. , Lunghi M. , Chiappino-Pepe A. , Waldman B.S. , Nicolas D. , Varesio E. , Hehl A. , Lourido S. , Hatzimanikatis V. , et al. (2020) **Functional and Computational Genomics Reveal Unprecedented Flexibility in Stage-Specific Toxoplasma Metabolism** *Cell Host Microbe* **27**:290–306

41. Li Z.H. , King T.P. , Ayong L. , Asady B. , Cai X. , Rahman T. , Vella S.A. , Coppens I. , Patel S. , Moreno S.N.J (2021) **A plastid two-pore channel essential for inter-organelle communication and growth of Toxoplasma gondii** *Nat Commun* **12**

42. Li Z.H. , Ramakrishnan S. , Striepen B. , Moreno S.N (2013) **Toxoplasma gondii relies on both host and parasite isoprenoids and can be rendered sensitive to atorvastatin** *PLoS Pathog* **9**

43. Liang X. , Cui J. , Yang X. , Xia N. , Li Y. , Zhao J. , Gupta N. , Shen B (2020) **Acquisition of exogenous fatty acids renders apicoplast-based biosynthesis dispensable in tachyzoites of Toxoplasma** *J Biol Chem* **295**:7743–7752

44. Lim L. , Linka M. , Mullin K.A. , Weber A.P. , McFadden G.I (2010) **The carbon and energy sources of the non-photosynthetic plastid in the malaria parasite** *FEBS Lett* **584**:549–554

45. Lim L. , McFadden G.I (2010) **The evolution, metabolism and functions of the apicoplast** *Philos Trans R Soc Lond B Biol Sci* **365**:749–763

46. Long S. , Anthony B. , Drewry L.L. , Sibley L.D (2017) **A conserved ankyrin repeat-containing protein regulates conoid stability, motility and cell invasion in Toxoplasma gondii** *Nat Commun* **8**

47. Long S. , Brown K.M. , Drewry L.L. , Anthony B. , Phan I.Q.H. , Sibley L.D (2017) **Calmodulin-like proteins localized to the conoid regulate motility and cell invasion by Toxoplasma gondii** *PLoS Pathog* **13**

48. Long S. , Brown K.M. , Sibley L.D (2018) **CRISPR-mediated Tagging with BirA Allows Proximity Labeling in Toxoplasma gondii** *Bio Protoc* **8**

49. Long S. , Wang Q. , Sibley L.D (2016) **Analysis of Noncanonical Calcium-Dependent Protein Kinases in Toxoplasma gondii by Targeted Gene Deletion Using CRISPR/Cas9** *Infect Immun* **84**:1262–1273

50. Low L.M. , Stanisic D.I. , Good M.F (2018) **Exploiting the apicoplast: apicoplast-targeting drugs and malaria vaccine development** *Microbes Infect* **20**:477–483

51. McFadden G.I. , Roos D.S (1999) **Apicomplexan plastids as drug targets** *Trends Microbiol* **7**:328–333

52. McFadden G.I. , Yeh E (2017) **The apicoplast: now you see it, now you don't** *Int J Parasitol* **47**:137–144

53. Mullin K.A. , Lim L. , Ralph S.A. , Spurck T.P. , Handman E. , McFadden G.I (2006) **Membrane transporters in the relict plastid of malaria parasites** *Proc Natl Acad Sci U S A* **103**:9572–9577

54. Niu Z. , Ye S. , Liu J. , Lyu M. , Xue L. , Li M. , Lyu C. , Zhao J. , Shen B (2022) **Two apicoplast dwelling glycolytic enzymes provide key substrates for metabolic pathways in the apicoplast and are critical for Toxoplasma growth** *PLoS Pathog* **18**

55. Obornik M. , Janouskovec J. , Chrudimsky T. , Lukes J (2009) **Evolution of the apicoplast and its hosts: from heterotrophy to autotrophy and back again** *Int J Parasitol* **39**:1–12

56. Pao S.S. , Paulsen I.T. , Saier M.H. (1998) **Major facilitator superfamily** *Microbiol Mol Biol Rev* **62**:1–34

57. Plattner F. , Soldati-Favre D (2008) **Hijacking of host cellular functions by the Apicomplexa** *Annu Rev Microbiol* **62**:471–487

58. Ralph S.A. , van Dooren G.G. , Waller R.F. , Crawford M.J. , Fraunholz M.J. , Foth B.J. , Tonkin C.J. , Roos D.S. , McFadden G.I. (2004) **Tropical infectious diseases: metabolic maps and functions of the Plasmodium falciparum apicoplast** *Nat Rev Microbiol* **2**:203–216

59. Ramakrishnan S. , Docampo M.D. , Macrae J.I. , Pujol F.M. , Brooks C.F. , van Dooren G.G. , Hiltunen J.K. , Kastaniotis A.J. , McConville M.J. , Striepen B. (2012) **Apicoplast and endoplasmic reticulum cooperate in fatty acid biosynthesis in apicomplexan parasite Toxoplasma gondii** *J Biol Chem* **287**:4957–4971

60. Salomaki E.D. , Kolisko M (2019) **There Is Treasure Everywhere: Reductive Plastid Evolution in Apicomplexa in Light of Their Close Relatives** *Biomolecules* **9**

61. Sayers C.P. , Mollard V. , Buchanan H.D. , McFadden G.I. , Goodman C.D (2018) **A genetic screen in rodent malaria parasites identifies five new apicoplast putative membrane transporters, one of which is essential in human malaria parasites** *Cell Microbiol* **20**

62. Sidik S.M. , Huet D. , Ganesan S.M. , Huynh M.H. , Wang T. , Nasamu A.S. , Thiru P. , Saeij J.P.J. , Carruthers V.B. , Niles J.C. , et al. (2016) **A Genome-wide CRISPR Screen in Toxoplasma Identifies Essential Apicomplexan Genes** *Cell* **166**:1423–1435

63. Sleda M.A. , Li Z.H. , Behera R. , Baierna B. , Li C. , Jumpathong J. , Malwal S.R. , Kawamukai M. , Oldfield E. , Moreno S.N.J (2022) **The Heptaprenyl Diphosphate Synthase (Coq1) Is the Target of a Lipophilic Bisphosphonate That Protects Mice against Toxoplasma gondii Infection** *mBio* **13**

64. Soldati D. , Boothroyd J.C (1993) **Transient transfection and expression in the obligate intracellular parasite Toxoplasma gondii** *Science* **260**:349–352

65. Striepen B (2011) **The apicoplast: a red alga in human parasites** *Essays Biochem* **51**:111–125

66. Swift R.P. , Rajaram K. , Keutcha C. , Liu H.B. , Kwan B. , Dziedzic A. , Jedlicka A.E. , Prigge S.T (2020) **The NTP generating activity of pyruvate kinase II is critical for apicoplast maintenance in Plasmodium falciparum** *Elife* **9**

67. Tjhin E.T. , Hayward J.A. , McFadden G.I. , van Dooren G.G. (2020) **Characterization of the apicoplast-localized enzyme TgUroD in Toxoplasma gondii reveals a key role of the apicoplast in heme biosynthesis** *J Biol Chem* **295**:1539–1550

68. Tyra H.M. , Linka M. , Weber A.P. , Bhattacharya D (2007) **Host origin of plastid solute transporters in the first photosynthetic eukaryotes** *Genome Biol* **8**

69. van Dooren G.G. , Tomova C. , Agrawal S. , Humbel B.M. , Striepen B. (2008) **Toxoplasma gondii Tic20 is essential for apicoplast protein import** *Proc Natl Acad Sci U S A* **105**:13574–13579

70. Vaughan A.M. , O'Neill M.T. , Tarun A.S. , Camargo N. , Phuong T.M. , Aly A.S. , Cowman A.F. , Kappe S.H (2009) **Type II fatty acid synthesis is essential only for malaria parasite late liver stage development** *Cell Microbiol* **11**:506–520

71. Waller R.F. , Keeling P.J. , Donald R.G. , Striepen B. , Handman E. , Lang-Unnasch N. , Cowman A.F. , Besra G.S. , Roos D.S. , McFadden G.I (1998) **Nuclear-encoded proteins target to the plastid in Toxoplasma gondii and Plasmodium falciparum** *Proc Natl Acad Sci U S A* **95**:12352–12357

72. Walmsley A.R. , Barrett M.P. , Bringaud F. , Gould G.W (1998) **Sugar transporters from bacteria, parasites and mammals: structure-activity relationships** *Trends Biochem Sci* **23**:476–481

73. Wan W. , Dong H. , Lai D.H. , Yang J. , He K. , Tang X. , Liu Q. , Hide G. , Zhu X.Q. , Sibley L.D. , et al. (2023) **The Toxoplasma micropore mediates endocytosis for selective nutrient salvage from host cell compartments** *Nat Commun* **14**

74. Weber A.P. , Linka M. , Bhattacharya D (2006) **Single, ancient origin of a plastid metabolite translocator family in Plantae from an endomembrane-derived ancestor** *Eukaryot Cell* **5**:609–612

75. Xia N. , Ye S. , Liang X. , Chen P. , Zhou Y. , Fang R. , Zhao J. , Gupta N. , Yang S. , Yuan J. , et al. (2019) **Pyruvate Homeostasis as a Determinant of Parasite Growth and Metabolic Plasticity in Toxoplasma gondii** *mBio* **10**

76. Yeh E. , DeRisi J.L (2011) **Chemical rescue of malaria parasites lacking an apicoplast defines organelle function in blood-stage Plasmodium falciparum** *PLoS Biol* **9**

77. Yesbolatova A. , Saito Y. , Kitamoto N. , Makino-Itou H. , Ajima R. , Nakano R. , Nakaoka H. , Fukui K. , Gamo K. , Tominari Y. , et al. (2020) **The auxin-inducible degron 2 technology provides sharp degradation control in yeast, mammalian cells, and mice** *Nat Commun* **11**

78. Zhang M. , Wang C. , Otto T.D. , Oberstaller J. , Liao X. , Adapa S.R. , Udenze K. , Bronner I.F. , Casandra D. , Mayho M. , et al. (2018) **Uncovering the essential genes of the human malaria parasite Plasmodium falciparum by saturation mutagenesis** *Science* **360**

79. Zuther E. , Johnson J.J. , Haselkorn R. , McLeod R. , Gornicki P (1999) **Growth of Toxoplasma gondii is inhibited by aryloxyphenoxypropionate herbicides targeting acetyl-CoA carboxylase** *Proc Natl Acad Sci U S A* **96**:13387–13392

Author information

Hui Dong

National Key Laboratory of Veterinary Public Health Security, College of Veterinary Medicine, China Agricultural University, Beijing 100193, China, National Animal Protozoa Laboratory and School of Veterinary Medicine, China Agricultural University, Beijing 100193, China

Kai He

National Key Laboratory of Veterinary Public Health Security, College of Veterinary Medicine, China Agricultural University, Beijing 100193, China, National Animal Protozoa Laboratory and School of Veterinary Medicine, China Agricultural University, Beijing 100193, China

Jiong Yang

State Key Laboratory of Biocontrol, School of Life Sciences, Sun Yat-Sen University, Guangzhou 510275, China

Wen-Bin Zheng

College of Veterinary Medicine, Shanxi Agricultural University, Taigu 030801, Shanxi Province, China

De-Hua Lai

State Key Laboratory of Biocontrol, School of Life Sciences, Sun Yat-Sen University, Guangzhou 510275, China

ORCID iD: 0000-0002-4709-1507

Jing Liu

National Key Laboratory of Veterinary Public Health Security, College of Veterinary Medicine, China Agricultural University, Beijing 100193, China, National Animal Protozoa Laboratory and School of Veterinary Medicine, China Agricultural University, Beijing 100193, China

Hui-Yong Ding

National Key Laboratory of Veterinary Public Health Security, College of Veterinary Medicine, China Agricultural University, Beijing 100193, China, National Animal Protozoa Laboratory and School of Veterinary Medicine, China Agricultural University, Beijing 100193, China

Rui-Bin Wu

National Key Laboratory of Veterinary Public Health Security, College of Veterinary Medicine, China Agricultural University, Beijing 100193, China, National Animal Protozoa Laboratory and School of Veterinary Medicine, China Agricultural University, Beijing 100193, China

Kevin M. Brown

Department of Microbiology and Immunology, University of Oklahoma Health Sciences Center, Oklahoma City, Oklahoma, USA

Geoff Hide

Biomedical Research and Innovation Centre and Environmental Research and Innovation Centre, School of Science, Engineering and Environment, University of Salford, Salford, M5 4WT, UK

ORCID iD: 0000-0002-3608-0175

Zhao-Rong Lun

State Key Laboratory of Biocontrol, School of Life Sciences, Sun Yat-Sen University, Guangzhou 510275, China

Xing-Quan Zhu

College of Veterinary Medicine, Shanxi Agricultural University, Taigu 030801, Shanxi Province, China

ORCID iD: 0000-0003-2530-4628

Shaojun Long

National Key Laboratory of Veterinary Public Health Security, College of Veterinary Medicine, China Agricultural University, Beijing 100193, China, National Animal Protozoa Laboratory and School of Veterinary Medicine, China Agricultural University, Beijing 100193, China

For correspondence: LongS2018@163.com

ORCID iD: 0000-0002-5409-2831

Editors

Reviewing Editor
Arturo Casadevall
Johns Hopkins Bloomberg School of Public Health, United States of America

Senior Editor
Detlef Weigel
Max Planck Institute for Biology Tübingen, Germany

Reviewer #1 (Public Review):

The apicoplast, a non-photosynthetic vestigial chloroplast, is a key metabolic organelle for the synthesis of certain lipids in apicomplexan parasites. Although it is clear metabolite exchange between the parasite cytosol and the apicoplast must occur, very few transporters associated with the apicoplast have been identified. The current study combines data from previous studies with new data from biotin proximity labeling to identify new apicoplast resident proteins including two putative monocarboxylate transporters termed MCT1 and MCT2. The authors conduct a thorough molecular phylogenetic analysis of the newly identified apicoplast proteins and they provide compelling evidence that MCT1 and MCT2 are necessary for normal growth and plaque formation in vitro along with maintenance of the apicoplast itself. They also provide indirect evidence for a possible need for these transporters in isoprenoid biosynthesis and fatty acid biosynthesis within the apicoplast. Finally, mouse infection experiments suggest that MCT1 and MCT2 are required for normal virulence, with MCT2 completely lacking at the administered dose. Overall, this study is generally of high quality, includes extensive quantitative data, and significantly advances the field by identifying several novel apicoplast proteins together with establishing a critical role for two putative transporters in the parasite. The study, however, could be further strengthened by addressing the following aspects:

Main comments
1. The conclusion that condition depletion of AMT1 and/or AMT2 affects apicoplast synthesis of IPP is only supported by indirect measurements (effects on host GFP uptake or trafficking, possibly due to effects on IPP dependent proteins such as rabs, and mitochondrial membrane potential, possibly due to effects on IPP dependent ubiquinone). This conclusion would be more strongly supported by directly measuring levels of IPP. If there are technical limitations that prevent direct measurement of IPP then the author should note such limitations and acknowledge in the discussion that the conclusion is based on indirect evidence.

2. The conclusion that condition depletion of AMT1 and/or AMT2 affects apicoplast synthesis of fatty acids is also poorly supported by the data. The authors do not distinguish between the lower fatty acid levels being due to reduced synthesis of fatty acids, reduced salvage of host fatty acids, or both. Indeed, the authors provide evidence that parasite endocytosis of GFP is dependent on AMT1 and AMT2. Host GFP likely enters the parasite within a membrane bound vesicle derived from the PVM. The PVM is known to harbor host-derived lipids. Hence, it is possible that some of the decrease in fatty acid levels could be due to reduced lipid salvage from the host. Experiments should be conducted to measure the synthesis and salvage of fatty acids (e.g., by metabolic flux analysis), or the authors should acknowledge that both could be affected.

Reviewer #2 (Public Review):

In this study Hui Dong et al. identified and characterized two transporters of the monocarboxylate family, which they called Apcimplexan monocarboxylate 1 and 2 (AMC1/2) that the authors suggest are involved in the trafficking of metabolites in the non-photosynthetic plastid (apicoplast) of Toxoplasma gondii (the parasitic agent of human toxoplasmosis) to maintain parasite survival. To do so they first identified novel apicoplast transporters by conducting proximity-dependent protein labeling (TurboID), using the sole known apicoplast transporter (TgAPT) as a bait. They chose two out of the three MFS transporters identified by their screen based and protein sequence similarity and confirmed apicoplast localisation. They generated inducible knock down parasite strains for both AMC1 and AMC2, and confirmed that both transporters are essential for parasite intracellular survival, replication, and for the proper activity of key apicoplast pathways requiring pyruvate as carbon sources (FASII and MEP/DOXP). Then they show that deletion of each protein induces a loss of the apicoplast, more marked for AMC2 and affects its morphology both at its four surrounding membranes level and accumulation of material in the apicoplast stroma. This study is very timely, as the apicoplast holds several important metabolic functions (FASII, IPP, LPA, Heme, Fe-S clusters...), which have been revealed and studied in depth but no further respective transporter have been identified thus far. hence, new studies that could reveal how the apicoplast can acquire and deliver all the key metabolites it deals with, will have strong impact for the parasitology community as well as for the plastid evolution communities. The current study is well initiated with appropriate approaches to identify two new putatively important apicoplast transporters, and showing how essential those are for parasite intracellular development and survival. However, in its current state, this is all the study provides at this point (i.e. essential apicoplast transporters disrupting apicoplast integrity, and indirectly its major functions, FASII and IPP, as any essential apicoplast protein disruption does). The study fails to deliver further message or function regarding AMC1 and 2, and thus validate their study. Currently, the manuscript just describes how AMC1/2 deletion impacts parasite survival without answering the key question about them: what do they transport? The authors yet have to perform key experiments that would reveal their metabolic function. I would thus recommend the authors work further and determine the function of AMC1 and 2.